Journal Pre-proofs

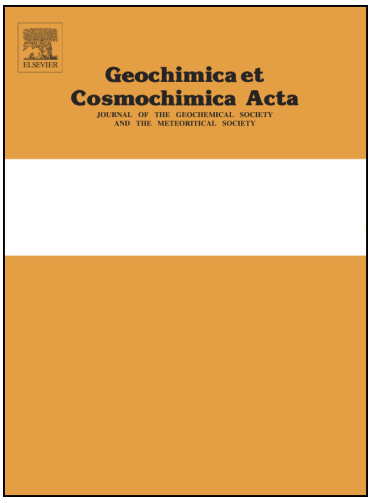

An experimental assessment of the chalcophile behavior of F, Cl, Br and I: implications for the fate of halogens during planetary accretion and the formation of magmatic ore deposits

E.S. Steenstra, F. van Haaster, R. van Mulligen, S. Flemetakis, J. Berndt, S. Klemme, W. van Westrenen

PII: S0016-7037(20)30017-X
DOI: https://doi.org/10.1016/j.gca.2020.01.006
Reference: GCA 11586

To appear in: *Geochimica et Cosmochimica Acta*

Received Date: 14 September 2019
Revised Date: 11 December 2019
Accepted Date: 6 January 2020

Please cite this article as: Steenstra, E.S., van Haaster, F., van Mulligen, R., Flemetakis, S., Berndt, J., Klemme, S., van Westrenen, W., An experimental assessment of the chalcophile behavior of F, Cl, Br and I: implications for the fate of halogens during planetary accretion and the formation of magmatic ore deposits, *Geochimica et Cosmochimica Acta* (2020), doi: https://doi.org/10.1016/j.gca.2020.01.006

An experimental assessment of the chalcophile behavior of F, Cl, Br and I: implications for the fate of halogens during planetary accretion and the formation of magmatic ore deposits

E.S. Steenstra[1–3]*, F. van Haaster[2], R. van Mulligen[2], S. Flemetakis[3], J. Berndt[3], S. Klemme[3], W. van Westrenen[2]

[1]*The Geophysical Laboratory, Carnegie Institution of Science, Washington D.C., the United States of America*

[2]*Faculty of Science, Vrije Universiteit Amsterdam, The Netherlands*

[3]*Institute of Mineralogy, University of Münster, Germany*

*Corresponding author: email address: esteenstra@carnegiescience.edu

ABSTRACT: The elemental and isotopic abundances of halogens (F, Cl, Br, I) are used to constrain planetary volatile loss and volatile delivery processes, but their behavior during magmatic differentiation in general, and sulfide liquid segregation in particular, is currently not well constrained. To test whether sulfide liquid segregation could affect halogen behavior during magmatic processes, we performed high-pressure experiments to systematically quantify the sulfide liquid - silicate melt partition coefficients ($D^{\text{sul liq}-\text{sil melt}}$ values, defined as the ratio between the wt.% concentration of the halogen in the sulfide liquid and silicate melt, respectively) of F, Cl, Br and I at a pressure of 1 GPa and temperatures of 1683–1883 K.

Results show that dry-polishing target surfaces is crucial for obtaining representative halogen concentrations of sulfide liquids. The results also show that no appreciable amounts of F partition into sulfide liquids, whereas Cl, Br and I behave increasingly chalcophile with increasing atomic radius (i.e., $D_{F}^{\text{sul liq}-\text{sil melt}} < D_{Cl}^{\text{sul liq}-\text{sil melt}} <$

$D_{Br}^{sul\ liq-sil\ melt} < D_{I}^{sul\ liq-sil\ melt}$), presumably as a result of an increasingly covalent nature of Fe-halogen bonds with increasing radius. This results in I behaving chalcophile ($D_{I}^{sul\ liq-sil\ melt}$ >1) in several experiments. In contrast to previous observations, $D_{Cl/Br}^{sul\ liq-sil\ melt}$ was found to be <1. The $D_{Cl,\ Br,\ I}^{sul\ liq-sil\ melt}$ predominantly vary with sulfide liquid melt composition, showing an increase with increasing O in the sulfide liquid, which itself is correlated with more oxidizing conditions (i.e., higher fO_2) or silicate melt FeO contents. The $D_{Cl,\ Br,\ I}^{sul\ liq-sil\ melt}$ values remain constant and/or potentially decrease again at the highest O concentrations of the sulfide liquids in this study (~2.5 wt.% O).

Results indicate that the magnitude of halogen depletions in the terrestrial, martian and lunar mantle are not strongly affected by segregation of sulfide liquids during their accretion, given the expected low modal abundance of sulfide liquids and/or relatively low $D_{Cl,\ Br,\ I}^{sul\ liq-sil\ melt}$ values. Core formation remains the most important process in establishing iodine depletion in the terrestrial mantle, whereas volatility-related loss seems most likely for F, Cl, Br and I, in case of the martian mantle. However, segregation of sulfide liquids during accretion could have resulted in a relative increase of the offset between the mantle depletions of the lighter and heavier halogens. The experimental results confirm the previously proposed feasibility of sulfide liquids as reservoirs for halogens in magmatic sulfide ore environments. As proposed by Mungall and Brenan (2003), fractional crystallization of these sulfide liquids in the absence of a silicate melt can lead to the formation of halide melts or fluids, consistent with the association between halide minerals and magmatic sulfide ores in some localities.

Keywords: volatile, halogens, core formation, accretion, sulfide

1. INTRODUCTION

Halogens are of key importance for understanding key aspects of volatile delivery and distribution processes during and after planetary accretion. For example, the abundance and isotopic composition of I in (extra)-terrestrial samples are used in ^{129}I - ^{129}Xe chronometry, which is widely applied to date the oldest (extra)-terrestrial samples (Gilmour et al., 2006). Absolute abundances of F and Cl and isotopic compositions have been used to argue for extensive post-accretion volatile loss from asteroid Vesta (Sarafian et al., 2017, 2019) and the Moon (Sharp et al., 2010; McCubbin et al., 2011; Hauri et al., 2015; Boyce et al., 2018; Stephant et al., 2019). On the other hand, the Cl systematics of Martian meteorites has been proposed to be dominated by later processes including fluid-brine interactions and/or assimilation-fractional crystallization (Williams et al., 2016). Halogens are also depleted in the terrestrial mantle, relative to putative bulk Earth compositions, with the heaviest halogens Br and I showing the highest depletions (Clay et al., 2017; Wang et al., 2018). Halogen depletions in the terrestrial mantle have also been related to extensive volatile loss during or following terrestrial differentiation (Sharp and Draper, 2013). In the case of I, its depletion may be enhanced through its preferential partitioning into the core (Jackson et al., 2018) and/or possibly in sulfide liquids that exsolved following solidification of the terrestrial magma ocean (O'Neill et al., 1991; Mungall and Brenan, 2003).

Sulfide liquids and sulfide minerals have been shown to be a significant sink for many trace elements, including nominally lithophile and siderophile elements, depending on the redox state and/or sulfide composition (Kiseeva and Wood, 2013; 2015; Wohlers and Wood, 2015, 2017; Steenstra et al., 2018, 2019). Although a role of

sulfides as a reservoir for mantle halogens, in particular I, has been considered for decades, the extent to which halogens partition into sulfide minerals or liquids is not well constrained. Goles and Anders (1961, 1962) proposed I to be weakly chalcophile on the basis of studies of iron meteorites. Hertogen et al. (1983) found evidence for preferential partitioning of Br into a sulfide mineral in enstatite chondrites, possibly niningerite or daubréelite, as Br concentrations were found to correlate strongly with Cd and Zn abundances. The presence of djerfisherite in aubrites suggests Cl may partition into sulfides at highly reducing conditions (Kimura et al., 1993). In case of Mercury, it has been suggested that Cl-bearing sulfides may be present at its surface, based on MESSENGER Gamma-Ray spectrometer data (Evans et al., 2015). Grossmann and Wasson (1985) found a significant correlation between abundances of chalcophile element Se and Br in chondrules of the LL chondrite Semarkona, suggesting Br was a chalcophile element in the chondrule precursors. Trace-element-rich evolved lunar melts such as KREEP basalts, felsites and monzogabbros were likely Cl (~0.8–1.7 wt.%) and F-rich (~0.5–1 wt.%) prior to major degassing events (McCubbin et al., 2011; 2015). Although most primitive lunar basalts are unlikely to have experienced saturation of a S-rich sulfide liquid (e.g., Steenstra et al., 2018, Day, 2018), highly differentiated lithologies including KREEP could have been sulfide liquid-saturated prior to eruption, as implied from the presence of trace amounts of sulfide phases (<0.6 modal %) in these samples (Simon et al., 1988; Neal and Kramer, 2003; Lin et al., 2012). In addition, Brenan et al. (2019) recently argued that some of the low-Ti basalts did experience sulfide saturation of a S-poor sulfde liquid. Segregated sulfide liquids may therefore have additionally depleted halogens in these samples.

Fuge and Johnson (1984) also suggested that I is a moderately chalcophile element, based on a comparison of compositions of co-existing sulfides and silicate materials from a range of geochemical environments. They reported analyses of terrestrial sulfides that contain up to 6 ppm I. The common occurrence of lawrencite $(Fe^{2+},Ni)Cl_2$ as an accessory phase in Fe-Ni alloy globules in lunar basalts and iron meteorites, as well as its occurrence in terrestrial magmatic sulfide deposits, suggests a potentially chalcophile nature for Cl (Mungall and Brenan, 2003). Mungall and Brenan (2003) also provided experimental evidence for a potential magmatic link between halide minerals and magmatic sulfide liquids in some ore deposits (e.g., the Sudbury Igneous Complex), suggesting the role of halogens in magmatic sulfide ores may be significant.

Peters et al. (1995) performed a preliminary study with the aim of quantifying I partitioning between sulfide liquids and silicate melts. They found that significant quantities of I can be incorporated in magmatic sulfide liquid. To further assess whether halogens indeed behave chalcophile, Mungall and Brenan (2003) performed a series of ambient- and high-pressure experiments in which sulfide liquids equilibrated with halogen-bearing silicate melts. They provided experimental evidence for the chalcophile nature of the halogens and observed increasingly chalcophile behavior with increasing atomic size of the halogen.

Several workers studied the potential siderophile behavior of the halogens. Armytage et al. (2013) studied the metal liquid - silicate melt partitioning behavior of I at high pressures (2–20 GPa) and temperatures (~2800 K) using a LHDAC (laser heated diamond anvil cell) technique. They found mildly siderophile behavior of I at all the investigated conditions, with metal liquid - silicate melt partition coefficients

($D_I^{\text{met liq}-\text{sil melt}}$) of ~0.6–4.3, depending of the composition of the Fe-rich alloy considered. Sharp and Draper (2013) performed three metal-silicate partitioning experiments at 15 GPa and 2173 K and found that Cl behaves highly incompatibly in S-poor, Fe-rich metal alloys. Kuwahara et al. (2017) performed similar metal liquid - silicate melt partitioning experiments from 4 to 23 GPa and 1923–2673 K and also found evidence for lithophile behavior of Cl. Jackson et al. (2018) used both LHDAC and piston-cylinder techniques to show that I may behave siderophile and/or chalcophile. A potential issue is that the experimental samples in most of the latter studies were prepared for analysis using oil/kerosene-based polishing techniques (Mungall and Brenan, 2003; Sharp and Draper, 2013; Kuwahara et al., 2017). This may have resulted in dissolution and/or re-distribution of halogens during polishing, given the unstable nature of halogens in sulfides (e.g., in the case of I; Jackson et al., 2018). The extent to which intrinsic variables may affect the halogen sulfide-silicate partitioning behavior are therefore not well constrained. Here, we present a systematic study describing the high-pressure sulfide liquid - silicate melt partitioning behavior of F, Cl, Br and I, at isobaric conditions (1 GPa) between 1673–1883 K, while using a single silicate melt composition and dry-polishing sample preparation techniques. The results are used to assess whether sulfide liquids may be a significant reservoir for halogens during planetary differentiation.

2. METHODS

2.1 High pressure-temperature experiments

High pressure-temperature experiments (summarized in Table 1) were performed in a Bristol-type end-loaded piston cylinder press at the high-pressure laboratory of the Vrije Universiteit Amsterdam. Two experiments (runs I-FeS-2 and 3) were performed using an identical press at the high-pressure laboratory of the Institute of Mineralogy, University of Münster. All experiments were performed at a pressure of 1 GPa at temperatures between 1683 and 1883 K using a ½ inch talc-pyrex cell assembly. The pressure calibration for this assembly was based on the fayalite + quartz = ferrosillite, albite = jadeite + quartz and $MgCr_2O_4 + SiO_2 = Cr_2O_3 + Mg_2SiO_4$ equilibria as well as the quartz-coesite transition (Bose and Ganguly, 1995; Klemme and O'Neill, 1997; Van Kan Parker et al., 2011). Experiments were conducted using a graphite-lined Pt capsule to minimize loss of halogens during the experiment. All experiments were performed using a synthetic equivalent of a primitive basalt (modeled after the Apollo 15 green glass; Steenstra et al., 2017). This composition was specifically chosen because we previously quantified sulfide liquid - silicate melt partition coefficients for this composition for a wide range of other elements (Steenstra et al., 2018; 2020a), allowing for direct comparison with the halogen partitioning results. Its relatively high initial FeO content makes this particular starting material also appropiate for the study of the distribution of halogens between sulfide liquids and silicate melts within intermediate- and late-stage magma ocean liquids on the Earth and Mars. The ground silicate starting material was doped with 1 to 2 wt.% I, 1 wt.% Cl, 2 wt.% Br and 1 or 4 wt.% F. Iodine was added to the silicate starting composition as KI, F as MgF_2, Cl as KCl and Br as KBr. Sulfides were

added to each experiment using stoichiometric FeS (99.5%, Alfa Aesar) and were packed in the bottom and top ends of the graphite capsule. The silicate powder was packed in between the two sulfide powder layers to reduce/prevent Pt contamination of the sulfide liquids (Wykes et al., 2015; Steenstra et al., 2018). Experimental run temperatures were monitored and controlled using a type D (97%W/3%Re - 75%W/25%Re) thermocouple and Eurotherm 2404 programmable controller. Samples were pressurized to 0.5 GPa and subsequently heated during which pressure was gradually increased to the target pressure. At 1073 K, samples were sintered for 45 to 60 min to reduce porosity of the graphite capsules and limit the infiltration of FeS into the graphite capsules at high temperatures. At peak temperatures, sulfide liquids and silicate melts were equilibrated for 15 to 300 min, depending on the target temperature (Table 1).

2.2 Electron microprobe analyses

Experimental run products were imbedded in ClaroFast® (i.e., methacrylate polymer, with low abundances (<1 wt.%) of Methyl methacrylate and dibenzoyl peroxide) or Struers Epofix® mounts using a Struers® mounting press. Samples were initially dry-polished using different grades of SiC sandpaper and graphite powder to prevent interaction of fluids / oils with the halogen-bearing sulfide liquids. Experimental charges were polished as shortly before EPMA analyses as possible (<24 hr, but usually only several hours), carbon coated and directly stored in a vacuum desiccator filled with nitrogen gas. Major element abundances in sulfide liquids and silicate melts were obtained using a JXA JEOL JXA-8530F electron probe microanalyser (EPMA) at the

University of Münster in wavelength-dispersive mode. Both sulfide liquids and silicate melts were analyzed using a defocused beam with beam diameters of 3–15 µm, depending of the size and texture of the measured phases. Major element abundances were determined using an accelerating voltage of 15 kV and a beam current of 20 nA. Counting times were 30 s for peak and 15 s for background for major elements. Sulfide liquid standards were tephroite for Mn, chalcopyrite for S and pure metal standards for Cr, Fe and Pt. Silicate melt standards were diopside for Si and Ca, forsterite for Mg, corundum for Al, hematite for Fe, tephroite for Mn, $KTiPO_5$ for K, TiO_2 for Ti, jadeite for Na, chalcopyrite for S and a pure metal standards for Cr. Standards for halogen analyses were Astimex Fluorite and Astimex Topaz for F, Astimex TlBrI for Br and I, and Astimex Tugtupite for Cl. These standard were initially ground using SiC and polished with aqueous 0.25 µm polishing fleece. Before carbon coating, all standards were cleaned with petroleum ether in an ultrasonic bath. All of the halogen standards were permanently stored under vacuum. Analysis of the Struers Epofix® mounting resin gave zero counts in terms of F, Br and I. The signal for Cl was 150 cps when measuring directly on the resin. However, measurements of Cl at the rim of a Cl-free phase gave a zero count rate, suggesting no issues arising from mounting resin fluorescence in terms of Cl.

Halogen abundances in the silicate melts and sulfide liquids were determined using an accelerating voltage of 15 kV and counting times of 120 seconds on peak and 60 seconds on background. Beam currents were 60 nA for glasses and 180 nA for sulfide liquids. These high beam currents and relatively long counting times were chosen specifically to further reduce halogen detection limits, as described and successfully

tested by Zhang et al. (2016, 2017). We show in the Appendix section A.1 that the use of such high beam currents does not result in halogen loss under the beam. The background for F was measured on the high-wavelength side only given the Fe*L*a interference on the low side. Measured concentrations of F, Br and I in the silicate melts were corrected for the overlap with Fe, Al and Ca (Zhang et al., 2016, 2017), respectively, using calibration curves based on measurements of nominally halogen-free glasses with variable FeO, Al_2O_3 and CaO concentrations. Fluorine contents in sulfides were corrected for the overlap with Fe according to the calibrated offset based on nominally F-free sulfides with variable Fe concentrations (Appendix section A.1). To control precision and accuracy, F, Cl and Br were routinely measured in well-characterized reference materials USNM Rhyolite VGA-568, NIST 610, USNM Makaopuhi A-99, USNM Juan da Fuca VG-2 and BCR2-G.

3.1 RESULTS

3.1 Run products

Typical experimental run products are shown in Fig. 1. The silicate melt usually quenched to a homogeneous glass, whereas lower temperature experiments crystallized olivine. This resulted in variations of silicate melt compositions, most notably in terms of MgO, Al_2O_3 and CaO concentrations (Table 2). In the majority of the experiments the initial vertical layering of sulfide liquid - silicate melt - sulfide liquid was retained. Due to this particular technique of sample loading, the reaction of the outer Pt capsule with sulfide liquid is reduced to a minimum, with Pt concentrations in sulfide liquids of generally less than 2 wt.% (Table 2). It should be noted that the addition of

such low quantities of Pt has no discernible effects on the activities of Fe, S and/or trace elements in the sulfide melts (Steenstra et al., 2018). Relative elemental distribution maps were obtained to assess the distribution of halogens in the quenched silicate and sulfide liquids. The maps do not show evidence for a high spatial correlation of halogens with any major compositional parameter, including oxygen (Fig. S.2–5). This suggests that the halogens in the sulfide liquids are present in the form of halides, instead of for example oxysulfide compounds. This would also be consistent with the strong correlation between Cl and Br - I contents of the sulfide liquids respectively (Fig. S.6). Experiments with high Cl contents of the sulfide liquid also have Cl-rich silicate melts, suggesting that equilibrium between both phases was established at high pressures and temperatures, as reflected by the consistent $\mathrm{D}_{\mathrm{Cl}}^{\mathrm{sul\ liq-sil\ melt}}$ values (Table 3). The correlation of Cl with Br or I contents therefore is not a result of the formation of halides following run product preparation.

3.2 Preferential loss of halogens from sulfide liquids during sample preparation

Given the fact that halogens are highly mobile in many liquids, care must be taken to apply appropiate sample polishing and -preparation techniques. To prevent erroneous results, all reported sulfide liquid - silicate melt partition coefficients ($\mathrm{D}_{i}^{\mathrm{sul\ liq-sil\ melt}}$, defined as the wt.% ratio of element *i* in the sulfide liquid and silicate melt, respectively) in this study are based on halogen sulfide liquid concentrations that were obtained by measuring the samples as soon as possible following sample preparation, dry-polishing and carbon-coating (<24 hours, but usually only after several hours). To assess to what extent sample polishing- and preparation techniques could affect $\mathrm{D}_{i}^{\mathrm{sul\ liq-sil\ melt}}$ values,

we re-analyzed I-bearing runs ESS-5 and FH-8 a second time after 7 months storage in a nitrogen desiccator. Subsequently these runs were polished wet (using both H_2O and oils) for assessment of the immediate effects of wet polishing on halogen mobility in the sulfide phases. The Br-bearing run FH-5, initially dry-polished, was stored in a nitrogen dessicator for 7 months and then polished wet immediately after retrieval from the desiccator.

The results show that Br and I concentrations for dry-polished samples remain constant (within error) after a 7 month storage interval (Fig. 2). This is consistent with the lack of visible coating-sample interaction, following the storage interval, suggesting no halogens dissolved or halides grew from the sulfide liquids within this time. However, subsequent wet repolishing using oils and H_2O results in a dramatic and consistent loss of halogens from the sulfide liquids, with abundances decreasing by up to an order magnitude (Fig. 2). It should be noted that Jackson et al. (2018) reported gradual loss of I from experimentally produced metal alloys. This discrepancy may be explained by the much higher pressures (up to 45 GPa) of the experiments of Jackson et al. (2018) and/or the potentially different nature of halogen storage in metal alloys compared to sulfide liquids at these pressures.

3.3 Assessment of mass balance and attainment of chemical equilibrium

Analyses of the experimental run products showed that post-experimental bulk F, Cl and I abundances are generally within error or higher than the added amounts (+75±42%, +17±30, –5±36 deviation relative to added amounts for Cl, F and I, respectively, Table S.1). Post-experimental measured abundances of Br are on average

slightly lower (–27±16) compared to initial abundances, which could point to some loss of Br during the experiment. The loss could have occurred during the sintering stage at 1073 K or, more likely, at peak conditions, perhaps through the formation of S-rich vapors and corresponding local melting of the Pt outer capsule (e.g., Wykes et al., 2015). Loss of Br could result in anomalous $\mathrm{D}_{i}^{\mathrm{sul\ liq-sil\ melt}}$ values, due to potentially different diffusion rates of Br in sulfide and silicate melts, respectively. Although diffusion rates of halogens in sulfide liquids are as of yet unconstrained, it has been demonstrated that diffusion rates of various other elements (e.g., Fe, Os, Pb) in sulfide minerals and -liquids are comparable to diffusion rates determined for basaltic melts (Brenan et al., 2000; Hart and Gaetani, 2006, and references therein). Figure S.7 shows the derived $\mathrm{D}_{\mathrm{Br,\ I}}^{\mathrm{sul\ liq-si\ melt}}$ plotted as a function of the % deviation of bulk halogen abundances relative to initial abundances and $\mathrm{D}_{\mathrm{Br,\ I}}^{\mathrm{sul\ liq-si\ melt}}$ values, suggesting our results are not affected by potential loss of Br and/or I. Most experiments were enriched in Cl, although Cl was not added in the original starting composition for some of these experiments. This is likely a result of Cl being present in the KI, KBr and MgF_2 powders as impurities. In the case of the experiments where only Cl was added, the consistently higher reconstructed post-experimental bulk abundances are most likely also related to this.

Previous studies from different research teams reported chemical equilibrium between silicate melt and sulfide liquid for a variety of trace elements with variable diffusion rates within 30 min at 1673–1773 K for experiments performed with capsules with similar dimensions as used in this study (Kiseeva and Wood, 2013, 2015; Steenstra et al., 2018). All experiments reported here were conducted for >30 min

(Table 1). Given that the diffusion rates of halogens in silicate melts are similar to diffusion rates for trace elements considered in these previous studies (Zhang et al., 2010), equilibrium between sulfide liquid and silicate melt should have been attained in all experiments. This agrees with the homogeneous distribution of halogens throughout the lower and upper segments of the silicate melts and with the well-defined correlation between $D_{O}^{\text{sul liq}-\text{si melt}}$ and $D_{\text{Cl, Br, F}}^{\text{sul liq}-\text{sil melt}}$ values (see section 3.4).

3.4 The sulfide liquid - silicate melt partitioning behavior of Cl, Br and I

To quantify the affinity of halogens with sulfide liquids, we consider the sulfide liquid - silicate melt partition coefficient ($D_{i}^{\text{sul liq}-\text{sil melt)}}$ (Table 1). A first major observation is that all $D_{F}^{\text{sul liq}-\text{sil melt}}$ values are very low, because all F concentrations in sulfide liquids are below the EPMA detection limits. This is consistent with the observations of Mungall and Brenan (2003). With increasing size, halogens become more compatible in sulfide liquids, with a relative sequence of $D_{F}^{\text{sul liq}-\text{sil melt}} < D_{Cl}^{\text{sul liq}-\text{sil melt}} < D_{Br}^{\text{sul liq}-\text{sil melt}} < D_{I}^{\text{sul liq}-\text{sil melt}}$. The log $D_{\text{Cl, Br, I}}^{\text{sul liq}-\text{sil melt}}$ values vary between –1.6 and –0.6, –0.8 and –0.4 and –0.2 and +0.3, respectively, where values of log $D_{\text{Cl, Br, I}}^{\text{sul liq}-\text{sil melt}} > 0$ reflect compatible behavior of the halogens in sulfide liquids. As proposed by Fuge and Johnson (1984), the increasingly compatible behavior of halogens in sulfide liquids in the latter sequence is most readily explained by an increasing covalent nature of Fe-halogen bonding with increasing atomic size. We note that Mungall and Brenan (2003) observed more chalcophile behavior of Cl relative to Br ($D_{\text{Cl/Br}}^{\text{sul liq}-\text{sil melt}}$ = 1.46), inconsistent with the

experimental data presented in this study where Cl and Br were simultaneously determined for the same experiment ($D_{Cl/Br}^{sul\ liq-sil\ melt}$ = 0.58±0.16; Table 3).

Figure 3 shows a compilation of the derived log $D_{Cl,\ Br,\ I}^{sul\ liq-sil\ melt}$ values from this study and the data of Mungall and Brenan (2003), plotted as a function of temperature. There are no clear effects of temperature on the sulfide liquid-silicate melt partitioning behavior of Cl, Br and I in our new experimental data set. However, the lower temperature $D_{Br,\ I}^{sul\ liq-sil\ melt}$ values of Mungall and Brenan (2003), and to a lesser extent $D_{Cl}^{sul\ liq-sil\ melt}$, are consistently lower than our measured $D_{Cl,\ Br,\ I}^{sul\ liq-sil\ melt}$ values (Fig. 3). This could point to positive temperature effects on $D_{Cl,\ Br,\ I}^{sul\ liq-sil\ melt}$. Unfortunately, the authors did not report O concentrations of the sulfide liquids in their experiments. The differences in $D_{Cl,\ Br,\ I}^{sul\ liq-sil\ melt}$ values could therefore be (in part) to different O concentrations of the sulfide liquids, as discussed later in this section. Another reason for the observed discrepancies is the use of water- and/or oil-based sample polishing techniques by Mungall and Brenan (2013) for some of their experiments, which could have resulted in preferential halogen loss from the sulfide liquids in these experiments (section 3.2), yielding lower $D_{Cl,\ Br,\ I}^{sul\ liq-sil\ melt}$ values. Overall, it is evident from Fig. 3 that there is considerable scatter of halogen sulfide liquid - silicate melt partition coefficients at a given temperature, suggesting temperature does not exert the major control on the variation of the halogen partitioning behavior between sulfide liquids and silicate melts.

Besides temperature, the major element compositions of the silicate melts also vary between experiments (SiO_2 = 43.25–53.05, Al_2O_3 = 3.87–12.30, CaO = 2.72–13.65, FeO = 2.74–12.79 and MgO = 11.64–25.79 wt.%). This is mostly due to variable

degrees of crystallization of olivine in lower temperature runs (e.g., FH-3) and because of slight variations in experimental redox states. Variations in silicate melt composition could affect the partitioning of trace elements between metals, sulfides and silicates (e.g., O'Neill and Eggins, 2002; Siebert et al., 2011; Steenstra et al., 2017). For example, Webster and De Vivo (2002) showed that the solubility of Cl in silicate melts strongly varies as a function of silicate melt composition. They found that the Ca, Mg and Fe contents of the silicate melt, and their role as network-modifying ions and/or as ions in charge balance with Al, control the solubility of Cl in silicate melts. Silicate melt compositional effects on solubility may also be significant for the other halogens (e.g., Dalou et al., 2015). However, strong silicate melt compositional effects on $\mathrm{D}_{\mathrm{Cl,\ Br,\ I}}^{\mathrm{sul\ liq-sil\ melt}}$ are not evident from our new data, with $\mathrm{D}_{\mathrm{Cl,\ Br,\ I}}^{\mathrm{sul\ liq-sil\ melt}}$ values being similar for the end-member silicate melt compositions.

It has also been hypothesized that halogen abundances in the silicate melt may also affect their own partitioning (Mungall and Brenan, 2003). Although it is widely established that Cl and other halogens affect the structure and physical properties of silicate melts (e.g., Zimova and Webb, 2006; Dalou et al., 2015) and therefore perhaps the partitioning of trace elements between silicate phases (Li and Hermann, 2017), halogen abundances themselves are inherently correlated with $\mathrm{D}_{\mathrm{Cl,\ Br,\ I}}^{\mathrm{sul\ liq-sil\ melt}}$. Because of the limited size of our new dataset, such effects cannot be accurately derived.

Figure 4 suggests that a significant fraction of the observed variability of $\mathrm{D}_{\mathrm{Cl,\ Br,\ I}}^{\mathrm{sul\ liq-sil\ melt}}$ can instead be explained by a strong correlation with $\mathrm{D}_{\mathrm{O}}^{\mathrm{sul\ liq-sil\ melt}}$. As the amount of O in the sulfide liquid is increased with increasing FeO concentration of the silicate melt (Kiseeva and Wood, 2013, 2015), the trends seen in Fig. 4 imply that at

increasingly oxidizing conditions Cl, I and possibly Br behave more compatible in sulfide liquids, and potentially similarly compatibly at high O (>2 wt.%) contents of the sulfide liquids. An important role of O for halogen activity in sulfide alloys is in agreement with the large positive effects of O on I activity in metal alloys at high *P-T* conditions reported by Jackson et al. (2018). Similar variability of $\mathrm{D}_{i}^{\mathrm{sul\ liq-sil\ melt}}$ as a function of FeO of the silicate melt (and O contents of the sulfide liquid) has also previously been observed for other anions, including Se and Te (Steenstra et al., 2018, 2020a,b). Although the chalcophile behavior of the halogens is likely affected by other parameters (e.g., *P, T*) in addition to sulfide liquid O content, these variables cannot be identified using the current experimental dataset. Future work should aim to further constrain the variability of $\mathrm{D}_{\mathrm{Cl,\ Br,\ I}}^{\mathrm{sul\ liq-sil\ melt}}$ as a function of *P-T* and composition.

Table 1 Experimental run conditions. All experiments were performed at a constant pressure of 1 GPa.

	T (K)	t (min)	Composition	Observed phases [a]	SCSS (ppm) [b]
I-FeS-2	1758	300	GG + 2 wt.% I	Gl(45), Fe-S(55)	2002(73) [c]
I-FeS-3	1683	300	GG + 2 wt.% I	Gl(20), Quench(20), Ol(10), Fe-S(50)	2908(112)
ESS-5	1833	60	GG + 2 wt.% I	Gl(40), Fe-S(60)	2129(186)
FH-8	1883	15	GG + 2 wt.% I	Gl(20), Quench(25), Fe-S(55)	3588(392)
FH-9	1683	45	GG + 2 wt.% I	Gl(30), Fe-S(60), Ol(10)	1632(62)
RM-9	1683	90	GG + 2 wt.% I	Gl(70), Fe-S(15), Ol(15)	1643(95)
RM-8	1683	60	GG + 2 wt.% I	Gl(65), Fe-S(15), Ol(20)	1261(77)
ESS-7	1683	90	GG + 1 wt.% Cl	Gl(50), Fe-S(25), Ol(25)	1433(117)
FH-2	1683	120	GG + 1 wt.% Cl	Gl(35), Fe-S(60), Ol(5)	1878(66)
FH-4	1783	60	GG + 1 wt.% Cl	Gl(15), Fe-S(85)	2502(218)
RM-11	1683	60	GG + 1 wt.% Cl	Gl(50), Fe-S(40), Ol(10)	1240(80)
RM-1	1683	60	GG + 4 wt.% F	Gl(65), Fe-S(15), Ol(20)	1846(434)
RM-2	1683	120	GG + 4 wt.% F	Gl(70), Fe-S(15), Ol(15)	1679(134)
FH-3	1683	30	GG + 1 wt.% F	Gl(35), Fe-S(65)	b.d.l.[d]
RM-6	1783	30	GG + 4 wt.% F	Gl(85), Fe-S(15)	1845(90)
FH-5	1683	50	GG + 2 wt.% Br	Gl(55), Fe-S(40), Ol(5)	1645(138)
FH-6	1733	45	GG + 2 wt.% Br	Gl(50), Fe-S(50)	1886(103)
FH-7	1833	30	GG + 2 wt.% Br	Gl(60), Fe-S(40)	2482(189)
RM-3	1783	45	GG + 2 wt.% Br	Gl(80), Fe-S(10), Ol(10)	1962(106)
RM-5	1683	120	GG + 2 wt.% Br	Gl(70), Fe-S(15), Ol(15)	1819(120)
RM-7	1883	15	GG + 2 wt.% Br	Gl(85), Fe-S(15)	2139(176)
RM-10	1683	60	GG + 2 wt.% Br	Gl(60), Fe-S(25), Ol(15)	2008(128)

[a] Phases observed in experimental run products [b] Sulfur concentration at sulfide liquid saturation of the silicate melt [c] Numbers in parentheses are 2 standard errors in terms of least digits cited [d] b.d.l. = below detection limit

Table 2 Composition of silicate melts and sulfide liquids determined by EPMA (in wt.%).

Run #	I-FeS-2	I-FeS-3	ESS-5	FH-8	FH-9	RM-8	RM-9	ESS-7	FH-2	FH-4	RM-11	RM-1
	N = 25 [a]	*N = 27*	*N = 14*	*N = 38*	*N = 16*	*N = 26*	*N = 26*	*N = 24*	*N = 27*	*N = 35*	*N = 24*	*N = 14*
Silicate melts												
MgO	19.43(6)[b]	19.53(17)	19.79(9)	18.38(32)	13.64(31)	13.16(30)	14.28(6)	11.64(18)	14.77(7)	17.71(82)	11.73(26)	17.29(99)
SiO_2	51.44(8)	51.24(12)	51.97(18)	47.81(24)	51.76(40)	52.40(27)	51.71(10)	49.71(20)	52.70(7)	48.72(38)	50.59(12)	43.25(93)
Al_2O_3	8.50(5)	8.17(2)	8.67(5)	7.86(6)	9.65(9)	12.30(24)	12.11(4)	11.66(8)	10.78(5)	8.11(17)	11.67(10)	10.09(32)
CaO	9.08(4)	8.97(5)	8.93(6)	8.39(6)	10.18(14)	12.51(15)	12.82(6)	12.38(14)	10.36(7)	8.16(57)	12.14(9)	13.65(107)
FeO	6.16(5)	5.72(3)	6.58(5)	12.79(10)	8.46(12)	4.07(8)	2.83(4)	5.68(7)	2.74(4)	9.97(25)	5.70(11)	7.31(11)
K_2O	0.60(1)	0.83(1)	0.61(2)	0.70(9)	1.02(4)	1.28(2)	1.15(1)	2.38(10)	2.71(2)	1.63(9)	2.53(6)	0.14(2)
Na_2O	0.10(1)	0.07(1)	0.18(1)	0.23(2)	0.36(2)	0.78(2)	0.84(2)	0.12(1)	0.90(1)	0.56(5)	0.54(3)	0.20(2)
Cr_2O_3	0.09(1)	0.10(1)	0.05(1)	0.10(1)	0.07(1)	0.19(2)	0.16(1)	0.06(1)	0.02(1)	0.04(1)	0.15(1)	0.12(3)
TiO_2	0.31(2)	0.37(1)	0.29(2)	0.27(2)	0.31(2)	0.48(3)	0.48(2)	0.39(2)	0.37(2)	0.24(2)	0.42(3)	0.35(4)
S	0.20(1)	0.30(1)	0.21(2)	0.35(3)	0.163(6)	0.13(1)	0.16(1)	0.14(1)	0.19(1)	0.25(2)	0.12(1)	0.18(4)
F	–	–	–	–	–	–	–	–	–	–	–	7.05(78)
Cl	0.06(1)	0.064(4)	0.098(1)	0.10(1)	0.22(2)	0.55(5)	0.64(1)	1.83(11)	1.61(1)	0.79(7)	1.86(5)	0.26(4)
Br	–	–	–	–	–	–	–	–	–	–	–	–
I	0.544(2)	0.66(4)	0.29(1)	0.28(3)	0.31(2)	0.91(1)	0.99(1)	–	–	–	–	–
Total	97.20(11)	96.14(24)	97.74(22)	97.37(19)	96.22(24)	98.90(21)	98.39(13)	96.11(25)	97.18(12)	96.28(25)	97.65(16)	100.31(39)
	N = 37	*N = 19*	*N = 16*	*N = 53*	*N = 40*	*N = 21*	*N = 24*	*N = 16*	*N = 32*	*N = 27*	*N = 29*	*N = 17*
Sulfide liquids												
Fe	59.90(22)	59.75(26)	59.29(35)	61.07(37)	60.68(23)	54.73(73)	56.01(27)	59.13(47)	53.72(111)	61.09(29)	57.62(65)	58.93(44)
S	36.21(23)	37.66(50)	33.82(45)	32.21(55)	34.27(19)	35.03(46)	35.17(24)	36.02(42)	34.34(59)	33.56(31)	34.95(39)	33.89(34)
O	1.15(16)	n.d.[c]	2.36(43)	3.15(49)	1.66(22)	1.34(40)	1.35(18)	0.87(36)	0.69(10)	2.10(27)	1.50(26)	1.91(22)
Pt	0.52(20)	b.d.l.[d]	0.61(24)	1.09(46)	0.96(33)	1.12(58)	1.18(25)	1.07(38)	8.26(188)	0.74(31)	2.18(125)	2.22(70)
Cr	0.26(2)	0.30(4)	0.12(3)	0.15(2)	0.12(1)	0.59(9)	1.02(3)	0.25(7)	0.08(1)	0.07(1)	0.38(9)	0.25(4)
K	–	–	–	0.04(1)	0.04(1)	0.19(7)	0.14(4)	0.03(2)	0.11(4)	0.04(1)	0.05(5)	0.008(4)
Mn	0.09(1)	0.08(1)	0.07(1)	0.07(1)	0.066(4)	0.18(1)	0.26(1)	0.08(1)	0.07(1)	0.05(1)	0.13(1)	0.08(1)
F	–	–	–	–	–	–	–	–	–	–	–	b.d.l.
Cl	0.0048(4)	0.013(2)	0.024(4)	0.018(3)	0.034(3)	0.16(5)	0.038(3)	0.040(2)	0.06(2)	0.13(2)	0.11(4)	0.034(4)
Br	–	–	–	–	–	–	–	–	–	–	–	–
I	0.61(15)	0.53(15)	0.33(6)	0.23(3)	0.35(4)	2.53(47)	0.87(12)	–	–	–	–	–
Total	99.43((31)	99.22(54)	96.78(37)	98.05(30)	98.20(21)	95.90(63)	96.12(20)	97.68(49)	97.36(48)	97.80(22)	97.00(36)	97.37(25)

	RM-2	FH-3	RM-6	FH-5	FH-6	FH-7	RM-3	RM-5	RM-7	RM-10
	N = 16	*N = 8*	*N = 19*	*N = 61*	*N = 21*	*N = 29*	*N = 16*	*N = 18*	*N = 18*	*N = 17*
Silicate melts										
MgO	19.62(20)	25.79(102)	23.42(13)	12.98(18)	15.20(14)	19.33(5)	18.64(7)	13.63(30)	18.21(7)	12.72(27)
SiO_2	45.19(49)	53.05(131)	45.90(13)	51.56(13)	50.78(34)	52.40(9)	50.50(10)	49.50(9)	49.67(15)	49.29(27)
Al_2O_3	7.93(6)	3.87(121)	6.96(2)	10.25(5)	8.93(6)	8.58(3)	8.78(6)	9.40(31)	8.63(3)	9.02(9)
CaO	8.87(24)	2.72(111)	8.28(7)	10.71(8)	9.24(7)	8.97(4)	9.43(7)	10.15(42)	9.09(5)	9.46(9)
FeO	8.54(15)	10.37(65)	7.80(7)	6.36(5)	8.30(40)	5.51(6)	5.09(3)	9.42(35)	6.55(7)	12.51(8)
K_2O	0.41(2)	0.05(4)	0.40(1)	1.70(2)	1.34(3)	0.97(1)	1.30(2)	1.13(3)	1.89(3)	1.22(8)
Na_2O	0.59(3)	0.03(3)	0.71(2)	0.47(1)	0.29(1)	0.36(1)	0.81(2)	1.03(2)	0.23(1)	0.48(3)
Cr_2O_3	0.39(2)	0.72(21)	0.26(2)	0.05(1)	0.09(1)	0.05(1)	0.28(2)	0.35(2)	0.16(1)	0.37(2)
TiO_2	0.27(2)	0.13(8)	0.22(2)	0.33(2)	0.26(2)	0.29(2)	0.32(3)	0.34(2)	0.27(2)	0.32(2)
S	0.17(1)	b.d.l.	0.18(1)	0.16(1)	0.19(1)	0.25(2)	0.20(1)	0.18(1)	0.21(2)	0.20(1)

F	3.91(9)	0.64(36)	3.78(4)	–	–	–	–	–	–	–
Cl	0.66(7)	0.02(1)	0.67(2)	0.34(1)	0.150(4)	0.206(1)	0.656(2)	0.97(4)	0.214(1)	0.72(5)
Br	–	–	–	0.80(1)	0.94(4)	0.538(2)	1.21(1)	0.95(1)	1.62(2)	1.36(8)
I	–	–	–	–	–	–	–	–	–	–
Total	96.65(20)	97.46(60)	98.68(13)	95.83(12)	95.81(18)	97.54(14)	97.36(13)	97.49(14)	96.90(16)	97.87(30)
	N = 16	*N = 29*	*N = 23*	*N = 24*	*N = 29*	*N = 33*	*N = 23*	*N = 20*	*N = 33*	*N = 18*
Sulfide liquids										
Fe	59.28(36)	61.03(33)	58.63(20)	60.47(25)	61.19(26)	53.25(95)	56.43(82)	57.52(51)	54.95(73)	58.62(82)
S	33.28(28)	35.44(54)	33.28(23)	34.36(29)	35.98(33)	32.75(55)	34.07(62)	32.52(81)	33.22(36)	33.11(81)
O	2.42(23)	1.52(46)	2.67(19)	1.43(25)	2.32(44)	1.28(24)	2.19(72)	2.72(66)	1.07(22)	2.35(71)
Pt	1.39(33)	0.40(15)	2.08(24)	0.47(10)	0.22(4)	10.23(165)	0.93(39)	1.51(40)	8.41(123)	0.87(36)
Cr	0.47(10)	0.16(4)	0.54(7)	0.13(1)	0.14(3)	0.17(2)	0.84(10)	0.78(39)	0.43(6)	0.50(37)
K	0.02(1)	0.009(4)	0.06(1)	0.03(1)	0.013(3)	0.04(1)	0.05(1)	0.06(1)	0.06(2)	0.01(1)
Mn	0.09(1)	0.07(1)	0.11(1)	0.06(1)	0.060(5)	0.07(1)	0.12(2)	0.09(1)	0.112(5)	0.07(1)
F	b.d.l.	b.d.l.	b.d.l.	–	–	–	–	–	–	–
Cl	0.14(6)	0.013(2)	0.17(2)	0.06(1)	0.03(1)	0.029(3)	0.26(9)	0.17(4)	0.019(4)	0.10(6)
Br	–	–	–	0.25(11)	0.33(6)	0.14(2)	0.46(14)	0.37(10)	0.28(5)	0.40(36)
I	–	–	–	–	–	–	–	–	–	–
Total	97.14(30)	98.09(31)	97.56(28)	97.31(26)	100.29(16)	97.99(33)	95.63(81)	95.76(43)	98.57(28)	96.06(59)

[a] Number of analyses [b] Numbers in parentheses are 2 standard errors in terms of least digits cited [c] n.d. = not determined [d] b.d.l. = below detection limit

Table 3 Experimentally determined $D_i^{\text{sul liq}-\text{sil melt}}$ (sulfide liquid - silicate melt partition coefficients of element *i,* where abundances of element *i* are in wt.%) values of O, Cl, Br and I for the various experiments. Fluorine contents of sulfides in all of the experiments performed with the F-bearing silicate starting composition were below detection limit.

	$D_O^{\text{sul liq}-\text{sil melt}}$	$D_{Cl}^{\text{sul liq}-\text{sil melt}}$	$D_{Br}^{\text{sul liq}-\text{sil melt}}$	$D_I^{\text{sul liq}-\text{sil melt}}$
I-FeS-2	0.026(4)[a]	0.082(8)	–	1.12(27)
I-FeS-3	0.0318(2)[b]	0.21(4)	–	0.82(28)
ESS-5	0.054(10)	0.24(5)	–	1.13(26)
FH-8	0.075(12)	0.19(5)	–	0.80(19)
FH-9	0.039(5)	0.16(3)	–	1.14(22)
RM-9	0.031(4)	0.059(5)	–	0.83(12)
RM-8	0.030(9)	0.30(12)	–	2.63(52)
ESS-7	0.021(9)	0.022(2)	–	–
FH-2	0.016(2)	0.037(15)	–	–
FH-4	0.050(6)	0.16(4)	–	–
RM-11	0.035(6)	0.059(21)	–	–
RM-1	0.047(5)	0.13(3)	–	–
RM-2	0.060(6)	0.21(11)	–	–
FH-3	0.034(10)	b.d.l.[c]	–	–
RM-6	0.064(5)	0.25(4)	–	–
FH-5	0.034(6)	0.17(4)	0.31(14)	–
FH-6	0.055(10)	0.18(4)	0.35(8)	–
FH-7	0.029(5)	0.14(1)	0.26(4)	–
RM-3	0.051(17)	0.39(14)	0.38(11)	–
RM-5	0.065(16)	0.17(5)	0.39(11)	–
RM-7	0.025(5)	0.086(19)	0.17(3)	–
RM-10	0.056(4)	0.13(9)	0.30(29)	–

[a] Numbers in parentheses propagated errors on D values in terms of least digits cited [b] O contents of sulfide liquid were calculated using the predictive model of Kiseeva and Wood (2013) [c] b.d.l. = below detection limit

Table 4 Reported and calculated halogen contents of the Earth, Mars and Moon and the putative sulfide liquids.

	F	Cl	Br	I
Earth				
Assumed $D_i^{sul\ liq-sil\ melt}$ value	–	0.20	0.40	1
Concentrations	**ppm**	**ppm**	**ppb**	**ppb**
bulk Earth [a]	13±4	163±88	195±68	37±12
Calculated BSE assuming Fe-rich metal and sulfide liquid segregation and non-siderophile and non-chalcophile behavior of halogens [b]	19±6	243±131	291±101	55±18
Calculated BSE assuming only Fe-rich metal segregation and non-siderophile behavior of halogens [c]	18±5	223±121	267±93	51±16
Measured BSE [d]	20±5	16±14	39±36	12±7
Sulfide liquid concentrations of halogens [e]	0	2.8±1.5	6.6±2.3	3.0±1.0
Measured BSE corrected for sulfide liquid extraction and chalcophile behavior [f]	20±5	18±16	44±41	14±9
Measured BSE corrected for core formation (chalcophile and siderophile behavior) [g]	– [h]	–	–	28±23
% depletion of BSE relative to bulk Earth by sulfide liquid extraction	0	1.1	2.0	5.4
% depletion of BSE relative to bulk Earth by sulfide- and Fe-rich liquid extraction	–	–	–	69
Mars				
Assumed $D_i^{sul\ liq-sil\ melt}$ value	–	0.20	0.40	1
Concentrations	**ppm**	**ppm**	**ppb**	**ppb**
bulk Mars [i]	89±56	303±183	1285±545	113±13
Calculated BSM assuming Fe-rich metal and sulfide liquid segregation and non-siderophile and non-chalcophile behavior of halogens [b]	119±75	404±244	1499±941	151±17
Calculated BSM assuming only Fe-rich metal segregation and non-siderophile behavior of halogens [c]	94±59	319±193	1319±540	119±14
Measured BSM [j]	21±13	32±9	191±58	36±22
Sulfide liquid concentrations of halogens [e]	0	19±12	136±47	30±4
Measured BSM corrected for sulfide liquid extraction and chalcophile behavior [f]	21±13	47±24	282±149	53±39
% depletion of BSM relative to bulk Mars by sulfide liquid extraction	0	3.4	6.9	13.1

[a] Taken from Wang et al. (2018) [b] Calculated hypothetical bulk silicate Earth (BSE) or bulk silicate Mars (BSM) concentrations after formation of a 33 mass% terrestrial core or 25 mass% Martian core. Core masses include the potential segregation of sulfide liquids during accretion (here assumed to be 6 and 20 mass% for Earth and Mars, respectively). Concentrations were calculated assuming the reported bulk Earth or bulk Mars concentrations while considering non-siderophile and non-chalcophile behavior of halogens [c] Calculated hypothetical bulk silicate Earth (BSE) or bulk silicate Mars (BSM) concentrations after formation of a 33 mass% terrestrial core or 25 mass% Martian core, but assuming non-siderophile behavior of halogens. Core mass fractions were thus corrected for modeled sulfide liquid modal abundances [d] Actual reported BSE abundances for various halogens based on previous literature estimates of primitive terrestrial lithologies (Wang et al., 2018 and references therein) [e] Calculated halogen budgets of segregated sulfide liquids [f] Halogen

abundances in the BSE and BSM corrected for sulfide liquid extraction (see section 4.1). Assumed modal abundances of sulfide liquids were considered to be 6 and 20 mass % for the Earth and Mars, respectively [g] Halogen abundances in the BSE corrected for sulfide liquid extraction and halogen partitioning into Fe-alloy during terrestrial core formation, assuming $D_{I}^{\text{met liq-sil melt}}$ = 3.4±1.1 [h] Potential effects of the formation of an Fe-rich terrestrial core on halogens could not be assessed for F, Cl and Br due to lack of $D_{i}^{\text{met liq-sil melt}}$ values [i] Based on bulk Mars estimates of Lodders and Fegley (1997) and Sanloup et al. (1999) [j] From Taylor (2013)

4. DISCUSSION

4.1 Effect of sulfide liquid segregation on planetary mantle halogen budgets during accretion

Halogens are depleted in the bulk silicate Earth (BSE) and in the bulk silicate Mars (BSM) relative to putative bulk Earth and bulk Mars compositions (e.g., Wang et al., 2018; Lodders and Fegley, 1997; Taylor, 2013). These depletions could reflect various episodes of volatility-related loss, for example during accretion of pre-cursor bodies (Hin et al., 2017; Norris and Wood, 2017) or during crystallization of their magma oceans (e.g., Dhaliwal et al., 2018). Halogen budgets may also have been affected by the late addition of a volatile-rich component to the Earth and Mars during the final stages of accretion (e.g., Wang and Becker, 2013).

The experimental results presented in this study show that a fraction of the terrestrial and martian mantle halogen budget may have partitioned into segregating sulfide liquids. The segregation of sulfide liquids has been proposed from volatile chalcophile element abundances and Mo/W ratios of the BSE (O'Neill, 1991; Wade et al., 2012; Wood et al., 2014; Savage et al., 2015) as well as from HSE systematics of martian nakhlite parent magmas (e.g., Mari et al., 2019). In addition, given the S-rich nature of the Martian core (e.g., Steenstra and van Westrenen, 2018 and references therein) S could have been transported to the core via sulfide liquids. Such sulfide liquids could have been removed from the terrestrial upper mantle and possibly migrated to the core during and/or after the final stages of terrestrial accretion (Wood et al., 2014) or perhaps ponded at intermediate depths in the terrestrial mantle. In both models equilibration between sulfide liquids and the silicate magma ocean would likely have occurred at relatively shallow levels in the terrestrial mantle, at oxygen fugacities that were likely

close to or within the range of that of the experiments presented here (Wood et al., 2014).

We use our new experimental results to assess the first-order potential of the extent of halogen depletion through sulfide liquid segregation. To estimate the potential $D_{Cl,\ Br,\ I}^{sul\ liq-sil\ melt}$ values during terrestrial differentiation, we assume that the FeO content of the residual magma ocean was the same as its current value of ~8 wt.% FeO. At an fO_2 of approximately the CCO buffer, this FeO content corresponds with an estimated O content of the Fe-rich sulfide liquid of ~2 wt.% (Kiseeva and Wood, 2013), equivalent to an estimated log $D_{O}^{sul\ liq-sil\ melt}$ value of ~ –1.3. We therefore estimate $D_{Cl,\ Br,\ I}^{sul\ liq-sil\ melt}$ to be close to the highest experimentally measured values, corresponding with the peak of the parabolic fits in Fig. (4) ($D_{Cl,\ Br,\ I}^{sul\ liq-sil\ melt}$ = ~0.2, 0.4 and 1, respectively). In case of Mars, the FeO content of the residual magma ocean was likely similar to its current mantle value of ~18.1±1.0 wt.% (Taylor, 2013), yielding potentially higher log $D_{O}^{sul\ liq-sil\ melt}$ values given the increase of O in sulfide melt with increasing FeO of the silicate melt (Kiseeva and Wood, 2013). However, given the more reduced state of the Martian interior (approx. –1 log unit below the iron-wüstite buffer or ΔIW; e.g., Rai and van Westrenen, 2013) and the reduced solubility of O in sulfide liquids with decreasing fO_2 (e.g., Fonseca et al., 2008), we assume that the $D_{Cl,\ Br,\ I}^{sul\ liq-sil\ melt}$ values assumed for terrestrial differentiation are comparable to those for Mars.

Assuming a contribution of ~2 wt.% S to the terrestrial core during the final 15% of Earth's accretion (Dreibus and Palme, 1996; Wood et al., 2014) or by means of sulfide liquid segregation in a terrestrial magma ocean (O'Neill, 1991) yields a modal

abundance of ~6 % FeS liquid. Using the estimated $D_{Cl,\ Br,\ I}^{sul\ liq-sil\ melt}$ values and assuming the bulk Earth abundances from Table 4 (Wang et al., 2018), we calculate that such a segregated FeS liquid would contain ~22 to 72 ppm Cl, ~72 to 149 ppb Br and ~34 to 67 ppb I. Due to the low modal abundance of sulfide liquids in the magma ocean inferred from S estimates of the terrestrial core (e.g., Dreibus and Palme, 1996; Suer et al., 2017), this reservoir would increase the true BSE abundances by only ~1.5 to 4.5 ppm for Cl, 5 to 9 ppb for Br and 2 to 4 ppb for I (Table 4). Figure 5 shows these results in comparison with predicted BSE abundances of halogens based on proposed bulk Earth compositions. The results show that halogen abundances are not significantly affected by segregation of sulfides during or following terrestrial accretion. Approximately 1, 2 and 5.5 % of the observed depletions of Cl, Br and I, respectively, can be explained by large-scale segregation of FeS liquids. Given the proposed siderophile behavior of I during core formation in the Earth ($D_{I}^{met\ liq-sil\ melt}$ = 3.4±1.1; Jackson et al., 2018), formation of a S-poor terrestrial core would additionally deplete I in the terrestrial mantle close to its estimated present-day mantle abundance (Fig. 5). Initial formation of a S-poor terrestrial core therefore exerts the major control on the depletion of I in the terrestrial magma ocean, compared to later sulfide liquid segregation in the residual magma ocean.

In case of Mars, we illustrate the effects of sulfide liquids on halogen mantle budgets by assuming a modal sulfide liquid abundance of 20 % during Martian differentiation, corresponding to the upper range of inferred S concentrations for the Martian core (~25 wt.% S; Khan and Connolly, 2008; Konopliv et al., 2011; Rai and van Westrenen, 2013; Steenstra and van Westrenen, 2018). In the latter model it is assumed that FeS liquid

saturation approximates the major core-mantle differentiation event in Mars. Consideration of these modal abundances of sulfide liquids results in depletions of the heavier halogens in the Martian mantle (Fig. 5). Segregation of 20 modal % of FeS liquid during differentiation of Mars explains 3.4, 6.9 and 13% of the Martian mantle depletions of Cl, Br and I, respectively. It should be noted that, according to the parameterization of Jackson et al. (2018), high-pressure formation of a Martian S-rich core would yield comparable or slightly higher $D_I^{\text{met liq}-\text{sil melt}}$ values (<3.5, calculated assuming the most S-rich scenario at 20 GPa).

The experimental results were also used to assess the potential role of sulfide liquids for incorporating halogens during magmatic differentiation of the Moon and Mercury. In case of the Moon, it is well established that S-rich sulfide liquid segregation could only (if at all) have occurred at the final (>85 %) stages of lunar magma ocean (LMO) crystallization (Morbidelli et al., 2018; Steenstra et al., 2019), as most primitive lunar magmas were not saturated in a S-rich sulfide liquid (Day, 2018; Steenstra et al., 2018, 2019). Despite the FeO-enrichment of the residual late-stage LMO liquid (>13–28 wt. % FeO, depending of the stage and the LMO crystallization model considered), O solubility in the putatitive S-rich sulfide melts must have been low due to low solubility of O (<0.5 wt.%; Fonseca et al., 2008) in Fe-S liquid at the reduced conditions of the LMO (ΔIW = ~ –2). Given this overall incompatible behavior of Cl, Br and I, the halogen concentrations of KREEP and other late-stage FeO-rich lunar melts remain largely unaffected by the putative late-stage segregation of sulfide liquids. If the LMO and/or lunar basalts experienced saturation by a S-poor sulfide liquid (Brenan et al., 2019), the estimated halogen depletion by sulfide fractionation would be more limited. This is due

to the increased incompatibility of I (and likely other halogens) in S-poor metal liquids (e.g., Jackson et al., 2018) and the very low proposed abundances of such sulfide phases (approx. 10 µg/g; Brenan et al., 2019). Similar results are expected for Vesta, given the similarly reduced state of the Vestan mantle and magmas (Toplis et al., 2013; Steenstra et al., 2016) and the absence of S-rich sulfide liquid saturation of non-cumulate eucrites (Steenstra et al., 2020b).

In case of accretion of highly reduced bodies such as Mercury and the aubrite parent body, the results show that partitioning of halogens in early, Fe-rich segregated sulfide liquids would have been negligible, as log $\mathrm{D}^{\mathrm{sul\ liq-sil\ melt}}_{\mathrm{Cl,\ Br,\ I}}$ decrease strongly with decreasing O of the sulfide liquid/decreasing fO_2 (Fig. 4). We therefore conclude that it is unlikely that the observed Cl abundance on Mercury's surface (Evans et al., 2015) stems from Cl-storage in Fe-rich sulfide liquids. However, halogens could be significantly more compatible in exotic sulfide phases such as alkali-rich sulfide minerals or Ca/Mg-rich sulfide liquids (Evans et al., 2015), which has not yet been experimentally assessed. Finally, it should be noted that all of the above calculations assume negligible effects of *P-T* on $\mathrm{D}^{\mathrm{sul\ liq-sil\ melt}}_{\mathrm{Cl,\ Br,\ I}}$, which may not be correct. For example, I behaves significantly more siderophile with increasing *P-T* (Jackson et al., 2018), suggesting that I partitioning between sulfide liquid and silicate melt may also be affected by pressure.

4.2 Nature of halogen depletions in planetary mantles

Although halogens behave slightly chalcophile to chalcophile, halogens are significantly more depleted in the terrestrial and martian mantle than would be expected given their $\mathrm{D}^{\mathrm{sul\ liq-sil\ melt}}_{\mathrm{Cl,\ Br,\ I}}$ values. Additional mantle depletions of halogens must therefore have

occurred through extraction of halogen-rich fluids, melts or brines to the terrestrial and/or martian crust given their hydrophilic nature (e.g., Kramers, 2003; Klemme, 2004; Kusebauch et al., 2015; Belluci et al., 2017), hydrodynamic escape or loss of the volatile veneer by large impactors (Kramers, 2003; Sharp and Draper, 2013; Clay et al., 2017) or perhaps due to core-mantle equilibration at high *P-T* in case of I in the Earth and potentially Mars (Armytage et al., 2013; Jackson et al., 2018; Fig. 5). Core formation depletion, however, is unlikely for Cl, which is highly incompatible in S-poor, Fe-rich liquids (Sharp and Draper, 2013; Kuwahara et al., 2017).

Due to the low *P-T* conditions of the lunar core-mantle boundary and the absence of significant quantities of sulfide liquids in the lunar interior, halogen lunar mantle depletions are expected to be predominantly related to degassing processes, perhaps through the formation of metal halides during the LMO stage (e.g., Sharp et al., 2010; Boyce et al., 2015). Our results do suggest that sulfide liquid segregation could have further enhanced the apparent more depleted nature of the heavier halogens in the terrestrial and martian mantle, relative to the expected volatility trend (Sharp and Draper, 2013; Taylor, 2013; Klemme and Stalder, 2018). On the other hand, Clay et al. (2017) concluded that the halogen depletion of the BSE is consistent with the depletions of lithophile elements with similar volatilities.

4.3 The fate of halogens in magmatic sulfide ore deposits

Halogen-rich minerals (e.g., halite, lawrencite) have been found in a variety of major magmatic sulfide ore deposits across the globe (see Mungall and Brenan, 2003 for a comprehensive review). This suggests that magmatic sulfide mineralization may be associated with halogen-bearing minerals. Mungall and Brenan (2003) hypothesized

that some of the sulfide liquids in magmatic sulfide ore deposits may have initially contained halogens. Mungall and Brenan (2003) provided experimental evidence that Cl (and likely by extension other halogens) are significantly fractionated between mono-sulfide solid solution (MSS) and sulfide liquids ($D_{Cl}^{MSS-sul\ liq}$ = 0.2). They thus argued that crystallization of an isolated magmatic sulfide liquid would be accompanied by a strong exclusion of Cl and potentially other halogens into a fluid or halide melt (Mungall and Brenan, 2003). As our results suggest comparable and usually higher solubilities of halogens in sulfide liquids, most notably Br and I (Fig. 3), our results are consistent with the hypothesis of Mungall and Brenan (2003) and confirm that magmatic sulfide liquids have significant halogen storage and transport capabilities (e.g., Hanley et al., 2008). Our results are, however, not consistent with the suggestion that exsolved fluid or halide melts exsolved from this sulfide liquid would be characterized by high Cl/Br ratios (Mungall and Brenan, 2003; Lecumberri-Sanchez and Bodnar, 2018), unless Br is significantly more compatible in MSS than Cl. Our results suggest that the opposite is expected (i.e., low Cl/Br of segregated fluid/halide melts, given the more chalcophile behavior of Br compared to Cl, Fig. 3–4). We conclude from the current experimental constraints that Cl/Br ratios are most likely not indicative of (a) sulfide liquid/MSS fractionation event(s), but we acknowledge that this should definitely be assessed in future sulfide liquid/MSS experiments containing both Br and Cl.

5. CONCLUSIONS

New experimental data shows that halogens potentially behave chalcophile during segregation of sulfide liquids following magma ocean solidification and/or subsequent magmatic events. The results show that the relative chalcophile behavior increases

from F > Cl > Br > I, with F concentrations in sulfide liquids below detection limit. This sequence can be readily explained by the replacement of the ionic nature of halogen bonding with more covalent-type bonding with increasing atomic size. Although significant quantities of halogens may be stored in sulfide liquids, segregation of sulfide liquids during the final stages of planetary accretion is most likely not a dominant process in establishing the proposed halogen depletions in planetary mantles.

Acknowledgements

This work was supported by a Carnegie Postdoctoral Fellowship to E.S.S., by a Netherlands Organization for Scientific Research (N.W.O.) Vici award to W.v.W and by SFG grant TRR-170. The majority of the reported experiments were performed by R.M. and F.H. as part of undergraduate research projects supervised by E.S.S. and W.v.W. First, we would like to thank G. Cody, N. Kueter and P. Ni for fruitful discussions. We also like to thank J. Brenan and two anonymous reviewers for their constructive comments that significantly improved the quality of the manuscript. We also thank J. Van Orman for editorial handling.

Research data

Research data related to this article can be accessed at (…).

References

Armytage R.M.G., Jephcoat A.P., Bouhifd M.A., Porcelli D. (2013) Metal-silicate partitioning of iodine at high pressures and temperatures: Implications for the Earth's core and 129*Xe budgets. *Earth Planet. Sci. Lett.* **373**, 140–149.

Bellucci J.J., Whitehouse M.J., John T., Nemchin A.A., Snape J.F., Bland P.A., Benedix G.K. (2017) Halogen and Cl isotopic systematics in Martian phosphates: Implications for the Cl cycle and surface halogen reservoirs on Mars. *Earth Planet. Sci. Lett.* **458,** 192–202.

Bose K. and Ganguly J. (1995) Experimental and theoretical studies of the stabilities of 630 talc, antigorite and phase A at high pressures with applications to subduction 631 processes. *Earth Planet. Sci. Lett.* **136**, 109–121.

Boyce J.W., Treiman A.H., Guan Y., Ma C., Eiler J.M., Gross J., Greenwood J.P., Stolper E.M. (2015) The chlorine isotope fingerprint of the lunar magma ocean. *Sci. Adv.* **1**, 8.

Boyce J.W., Kanee S.A., McCubbin F.M., Barnes J.J., Bricker H., Treiman A.H. (2018) Early loss, fractionation, and redistribution of chlorine in the Moon as revealed by the low-Ti lunar mare basalt suite. *Earth Planet. Sci. Lett.* **500**, 205–214.

Brenan J. M., Cherniak D.J., Rose L.A. (2000) Diffusion of osmium in pyrrhotite and pyrite: implications for closure of the Re-Os isotopic system. *Earth Planet. Sci. Lett.* **180,** 399–413.

Brenan J. M., Mungall J. E., Bennet N. R. (2019) Abundance of highly siderophile elements in lunar basalts controlled by iron sulfide melts. *Nat. Geosci.* **12**, 701–706.

Clay P.L., Burgess R., Busemann H., Ruzie-Hamilton L., Joachim B., Day J.M.D., Ballentine C.J. (2017) Halogens in chondritic meteorites and terrestrial accretion. *Nature* 551, 614–618.

Dalou C., Le Losq C., Mysen B.O., Cody G.D. (2015) Solubility and solution mechanisms of chlorine and fluorine in aluminosilicate melts at high pressure and high temperature. *Am. Mineral.* **100(10),** 2272–2283.

Day J.M.D. (2018) Geochemical constraints on residual metal and sulfide in the sources of lunar mare basalts. *Am. Mineral.* **103(11),** 1734–1740.

Dhaliwal J.K., Day J.M.D., Moynier F. (2018) Volatile element loss during planetary magma ocean phases. *Icarus* **300,** 249–260.

Dreibus G., Palme H. (1996) Cosmochemical constraints on the sulfur content in the Earth's core. GCA 60, 1125–1130.

Evans L.G., Peplowski P.N., McCubbin F.M., McCoy T.J., Nittler L.R., Zolotov M.Y., Ebel D.S., Lawrence D.J., Starr R.D., Weider S.Z., Solomon S.C. (2015) Chlorine on the surface of Mercury: MESSENGER gamma-ray measurements and implications for the planet's formation and evolution. *Icarus* **257**, 417–427.

Fonseca R.O.C., Campbell I.A., O'Neill H. St. C., Fitzgerald J. D. (2008) Oxygen solubility and speciation in sulphide-rich mattes. *Geochim. Cosmochim. Acta* **72,** 2619–2635.

Fuge R., Johnson C.C. (1984) Evidence for the chalcophile nature of iodine. *Chem. Geol.* **43**, 347–352.

Gilmour J.D., Pravdivtseva O.V., Busfield A., Hohenberg C.M. (2006) The I-Xe chronometer and the early solar system. *Meteorit. Planet. Sci.* **41**, 19–31.

Goles G.G., Anders E. (1961) On the geochemical character of iodine in meteorites. *J. Geophys. Res.* **66,** 3075–3077.

Goles G.G., Anders E. (1962) Abundance of iodine, tellurium, and uranium in meteorites. *Geochim. Cosmochim. Acta* **26**, 723–737.

Grossman J.N., Wasson J.T. (1985) The origin and history of the metal and sulfide components of chondrules. *Geochim. Cosmochim. Acta* **49**, 925–939.

Hanley J.J., Mungall J.E., Pettke T., Spooner E.T.C. and Bray C.J. (2008) Fluid and halide melt inclusions of magmatic origin in the ultramafic and lower banded series, Stillwater Complex, Montana, USA. *J. Petrol.* **49,** 1133–1160.

Hart S. R., Gaetani G. A. (2006) Mantle Pb paradoxes: the sulfide solution. *Contrib. Mineral. Petrol.* **152,** 295–308.

Hauri E.H., Weinreich T., Saal A.E., Rutherford M.C., van Orman J.A. (2011) High pre-eruptive water contents preserved in lunar melt inclusions. *Science* **333**, 213–215.

Hertogen J., Janssens M.-J., Takahashi H., Morgan J.W., Anders E. (1983) Enstatite chondrites: Trace element clues to their origin. *Geochim. Cosmochim. Acta* **47,** 2241–2255.

Hin R.C., Coath C.D., Carter P.J., Nimmo F., Lai Y.-J., Pogge von Strandmann P.A.E., Willbold M., Leinhardt Z.M., Walter M.J., Elliot T. (2017) Magnesium isotope evidence that accretional vapour loss shapes planetary compositions. *Nature* **549**, 511–515.

Jackson C.R.M., Bennett N.R., Du Z., Cottrell E., Fei Y. (2018) Early episodes of high-pressure core formation preserved in plume mantle. *Nature* **553**, 491–495.

Khan A., Connolly J.A.D. (2008) Constraining the composition and thermal state of Mars from inversion of geophysical data. *J. Geophys. Res.* **113,** E07003, doi:10.1029/2007JE002996.

Kimura M., Lin Y.-T., Ikeda Y., El Goresy A., Yanai K., Kojima H. (1993) Mineralogy of Antarctic aubrites, Yamato-793592 and Allan Hills-78113: Comparison with non-Antarctic aubrites and E-chondrites. *Proc. NIPR Symp. Antarct. Met.* **6**, 186–203.

Kiseeva E.S., Wood B.J. (2013) A simple model for chalcophile element partitioning between silicate and sulphide liquids with geochemical applications. *Earth Planet. Sci. Lett.* **383,** 68–81.

Kiseeva E.S., Wood B.J. (2015) The effects of composition and temperature on chalcophile and lithophile element partitioning into magmatic sulphides. *Earth Planet. Sci. Lett.* **424**, 280–294.

Klemme S. and O'Neill H. S. (1997) The reaction $MgCr_2O_4 + SiO_2 = Cr_2O_3 + MgSiO_3$ and the free energy of formation of magnesiochromite ($MgCr_2O_4$). *Contrib. Mineral. Petrol.* **130,** 59–65.

Klemme S. (2004) Evidence for fluoride melts in Earth's mantle formed by liquid immiscibility. *Geology* **32(5),** 441–444.

Konopliv A.S., Asmar S.W., Folkner W.M., Karatekin O., Nunes D.C., Smrekar S.E., Yoder C.F., Zuber M.T. (2011) Mars high resolution gravity fields from MRO, Mars seasonal gravity, and other dynamical parameters. *Icarus* **211,** 401–428.

Kramers J.D. (2003) Volatile element abundance patterns and an early liquid water ocean on Earth. *Precambrian Res.* **126**, 379–394.

Kusebauch C., John T., Whitehouse M.J., Klemme S., Putnis A. (2015) Distribution of halogens between fluid and apatite during fluid-mediated replacement processes. *Geochim. Cosmochim. Acta* **170,** 225–246.

Kuwahara H., Gotou H., Shinmei T., Ogawa N., Yamaguchi A., Takahata N., Sano Y., Yagi T., Sugita S. (2017) High pressure experiments on metal-silicate partitioning of chlorine in a magma ocean: Implications for terrestrial chlorine depletion. *Geochem. Geophys. Geosyst.* **18(11),** 3929–3945.

Li H., Hermann J. (2017) The effect of fluorine and chlorine on trace element partitioning between apatite and sediment melt at subduction zone conditions. *Chem. Geol.* **473,** 55–73.

Lin Y., Shen W., Liu Y., Xu L., Hofmann B.A., Mao Q., Tang G.Q., Wu F., Li X.H. (2012) Very high-K KREEP-rich clasts in the impact melt breccia of the lunar meteorite SaU 169: New constraints on the last residue of the Lunar Magma Ocean. *Geochim. Cosmochim. Acta* **85**, 19–40.

Lodders K., Fegley Jr B. (1997) An oxygen isotope model for the composition of Mars. *Icarus* **126**, 373–394.

Mari N., Riches A.J.V., Hallis L.J., Marrocchi Y., Villeneuve J., Gleissner P., Becker H., Lee M.R. (2019) Syneruptive incorporation of martian surface sulphur in the nakhlite lava flows revealed by S and Os isotopes and highly siderophile elements: implications for mantle sources in Mars. *Geochim. Cosmochim. Acta,* https://doi.org/10.1016/j.gca.2019.05.025

McCubbin F.M., Jolliff B.L., Nekvasil H., Carpenter P.K., Zeigler R.A., Steele A., Elardo S.M., Lindsley D.H. (2011) Fluorine and chlorine abundances in lunar apatites:

Implications for heterogeneous distributions of magmatic volatiles in the lunar interior. *Geochim. Cosmochim. Act.* **75,** 5073–5093.

McCubbin F.M., Vander Kaaden K.E., Tartèse R., Klima R.L., Liu Y., Mortimer J., Barnes J.J., Shearer C.K., Treiman A.H., Lawrence D.J., Elardo S.M., Hurley D.M., Boyce J.W., Anand M. (2015) Magmatic volatiles (H, C, N, F, S, Cl) in the lunar mantle, crust, and regolith: Abundances, distributions, processes, and reservoirs. *Am. Mineral.* **100,** 1668–1707.

Morbidelli A., Nesvorny D., Laurenz V., Marchi S., Rubie D.C., Elkins-Tanton L., Wieczorek M., Jacobson S. (2018) The timeline of the Lunar bombardment – revisited. *Icarus* **305,** 262–276.

Mungall J.E., Brenan J.M. (2003) Experimental evidence for the chalcophile behavior of the halogens. *Can. Min.* **41**, 207–220.

Neal C.R., Kramer G. (2003) The composition of KREEP: a detailed study of KREEP basalt 15386. **34th** *LPSC* #2023 (abstr.).

Norris C.A., Wood B.J. (2017) Earth's volatile contents established by melting and vaporization. *Nature* **549**, 507–510

O'Neill H.S.C. (1991) The origin of the Moon and the early history of the Earth – A chemical model. Part 2: The Earth. *Geochim. Cosmochim. Act* **55**, 1159–1172.

O'Neill H.S.C., Eggins S.M. (2002) The effect of melt composition on trace element partitioning: an experimental investigation of the activity coefficients of FeO, NiO, CoO, MoO_2 and MoO_3 in silicate melts. *Chem. Geol.* **186,** 151–181.

Peters M.T., Baker M.B., Burnett D.S. (1995) The partitioning of iodine between sulfide liquid and silicate liquid: implications for the cosmochemistry of iodine. **26th** *LPSC* #1558 (abstr.).

Rai N., van Westrenen W. (2013) Core-mantle differentiation in Mars. *J. Geophys. Res.: Planets* **118**, 1195–1203.

Sanloup C., Jambon A., Gille P. (1999) A simple chondritic model of Mars. *Phys. Earth. Planet. Int.* **112,** 43–54.

Sarafian A.R., John T., Roszjar J., Whitehouse M.J. (2017) Chlorine and hydrogen degassing in Vesta's magma ocean. *Earth Planet. Sci. Lett.* **459,** 311–319.

Sarafian A.R., Nielsen S.G., Marschall H.R., Gaetani G.A., Righter K., Berger E.L. (2019) The water and fluorine content of 4 Vesta. *Geochim. Cosmochim. Acta,* https://doi.org/10.1016/j.gca.2019.08.023.

Savage P.S., Moynier F., Chen H., Shofner G., Siebert J., Badro J., Puchtel I.S. (2015) Copper isotope evidence for large-scale sulphide fractionation during Earth's differentiation. *Geochem. Persp. Lett.* **I**, 53–64.

Sharp Z.D., Shearer C.K., McKeegan K.D., Barnes J.D., Wang Y.G. (2010) The chlorine isotope composition of the Moon and implications for an anhydrous mantle. *Science* **329**, 1050–1053.

Sharp Z.D., Draper D.S. (2013) The chlorine abundance of Earth: Implications for a habitable planet. *Earth Planet. Sci. Lett.* **369–370**, 71–77.

Siebert J., Corgne A., Ryerson F.J. (2011) Systematics of metal-silicate partitioning for many siderophile elements applied to Earth's core formation. *Geochim. Cosmochim. Acta* **75**, 1451–1489.

Simon S.B., Papike J.J., Laul J.C. (1988) Chemistry and petrology of the Apennine Front, Apollo 15. I - KREEP basalts and plutonic rocks. **18th** *LPSC,* 187–201.

Steenstra E.S., van Westrenen W. (2018) A synthesis of geochemical constraints on the inventory of light elements in the core of Mars. *Icarus* **315**, 69–78

Steenstra E.S., Knibbe J.S., Rai N., van Westrenen W. (2016) Constraints on core formation in Vesta from metal-silicate partitioning of siderophile elements. *Geochim. Cosmochim. Acta* **177**, 48–61.

Steenstra E.S., Lin Y.H., Dankers D., Rai N., Berndt J., Matveev S., van Westrenen W. (2017a) The lunar core can be a major reservoir for volatile elements S, Se, Te and Sb. *Sci. Rep.* **7,** 14552.

Steenstra E.S., Sitabi A.B., Lin Y.H., Rai N., Knibbe J.S., Berndt J., Matveev S., van Westrenen W. (2017b) The effect of melt composition on metal-silicate partitioning of siderophile elements and constraints on core formation in the angrite parent body. *Geochim. Cosmochim. Acta* **212**, 62–83

Steenstra E.S., Seegers A.X., Eising J., Tomassen B.G.J., Webers F.P.F., Berndt J., Klemme S., Matveev S., van Westrenen W. (2018) Evidence for a sulfur-undersaturated lunar interior from the solubility of sulfur in lunar melts and sulfide-silicate partitioning of siderophile elements. *Geochim. Cosmochim. Acta* **231**, 130–156.

Steenstra E.S., Berndt J., Rohrbach A., Klemme S., van Westrenen W. (2019) The fate of sulfur and chalcophile elements during crystallization of the lunar magma ocean. *LPSC* **50th,** #1137 (abstr.).

Steenstra E.S., Trautner V.T., Berndt J., Klemme S. and van Westrenen W. (2020a) Trace element partitioning between sulfides, metals and silicate melts at highly reduced conditions: insights into the depletion of volatile elements during core formation in recodes bodies. *Icarus,* **335,** 113408.

Steenstra E.S., Berndt J., Klemme S., Rohrbach A., Bullock E.S., van Westrenen W. (2020b) An experimental assessment of the potential of sulfide saturation of the source regions of eucrites and angrites: implications for asteroidal models of core formation, late accretion and volatile element depletions. *Geochim. Cosmochim. Acta* **269,** 39–62.

Stephant A., Anand M., Zhao X., Chan Q.H.S., Bonifacie M., Franchi I.A. (2019) The chlorine isotopic composition of the Moon: Insights from melt inclusions. *Earth Planet. Sci. Lett.* **523,** 115715.

Suer T.A., Siebert J., Laurent R., Menguy N., Guillaume F. (2017) A sulfur-poor terrestrial core inferred from metal-silicate partitioning experiments. *Earth Planet. Sci. Lett.* **469,** 84–97.

Taylor G.J. (2013) The bulk composition of Mars. *Chemie der Erde* **73,** 401–420.

Toplis M.J., Mizzon H., Monnereau M., Forni O., McSween H.Y., Mittlefehldt D.W., McCoy T.J., Prettyman T.H., De Sanctis M.C., Raymond C.A., Russell C.T. (2013) Chondritic models of 4 Vesta: Implications for geochemical and geophysical properties. *Meteorit. Planet. Sci.* **48**, 2300–2315.

van Kan Parker M., Mason P.R.D., van Westrenen W. (2011) Experimental study of trace element partitioning between lunar orthopyroxene and anhydrous silicate melt: Effects of lithium and iron. *Chem. Geol.* **285**, 1–14.

Wade J., Wood B.J., Tuff J. (2012) Metal-silicate partitioning of Mo and W at high pressures and temperatures: Evidence for late accretion of sulphur to the Earth. *Geochim. Cosmochim. Acta* **85**, 58–74

Wang H.S., Lineweaver C.H., Ireland T.R. (2018) The elemental abundances (with uncertainties) of the most Earth-like planet. *Icarus* **299**, 460–474.

Wang Z., Becker H. (2013) Ratios of S, Se and Te in the silicate Earth require a volatile-rich late veneer. *Nature* **499**, 328–331.\

Webster J.D., De Vivo B. (2002) Experimental and modeled solubilities of chlorine in aluminosilicate melts, consequences of magma evolution, and implications for exsolution of hydrous chloride melt at Mt. Somma-Vesuvius. *Am. Mineral.* **87,** 1046–1061.

Williams J.T., Shearer C.K., Sharp Z.D., Burger P.V., McCubbin F.M., Santos A.R., Agee C.B., McKeegan K.D. (2016) The chlorine isotopic composition of Martian meteorites 1: Chlorine isotope composition of Martian mantle and crustal reservoirs and their interactions. *Meteorit. Planet. Sci.* **51**, 2092–2110.

Wohlers A., Wood B.J. (2015) A Mercury-like component of early Earth yields uranium in the core and high mantle 142Nd. *Nature* **520,** 337–340.

Wohlers A., Wood B.J. (2017) Uranium, thorium and REE partitioning into sulfide liquids: Implications for reduced S-rich bodies. *Geochim. Cosmochim. Acta* **205**, 226–244.

Wood B.J., Kiseeva E.S., Mirolo F.J. (2014) Accretion and core formation: The effects of sulfur on metal-silicate partition coefficients. *Geochim. Cosmochim. Acta* **145**, 248–267.

Wykes J.L., O'Neill H.S.C., Mavrogenes J.A. (2015) The effect of FeO on the sulfur content at sulfide saturation (SCSS) and the selenium content at selenide saturation of silicate melts. *J. Petrol.* **56**, 1407–1424.

Zhang C., Koepke J., Wang L.-X., Wolff P.E., Wilke S., Stechern A., Almeev R., Holtz F. (2016) A Practical Method for Accurate Measurement of Trace Level Fluorine in Mg- and Fe-Bearing Minerals and Glasses Using Electron Probe Microanalysis. *Geost. Geoanal. Res.* **40**, 351–363.

Zhang C., Lin J., Pan Y., Feng R., Almeev R.R., Holz F. (2017) Electron Probe Microanalysis of Bromine in Minerals and Glasses with Correction for Spectral Interference from Aluminium, and Comparison with Microbeam Synchrotron X-Ray Fluorescence Spectrometry. *Geost. Geoanal. Res.* doi:10.1111/ggr.12169.

Zhang Y., Ni H., Chen Y. (2010) Diffusion data in silicate melts. *Rev. Mineral. Geochem*. **72**, 311–408

Zimova M., Webb S. (2006) The effect of chlorine on the viscosity of Na2O-Fe2O3-Al2O3-SiO2 melts. *Am. Mineral.* **91(2–3),** 344–352.

Figure captions

Fig. 1. Backscattered electron images of experimental run products (experiments FH-8, RM-8, RM-9).

Fig. 2. The abundance of Br and I in sulfide liquids as a function of the timing of EPMA analyses after polishing/sample preparation and of the used sample preparation techniques. If dry polished, halogen-bearing sulfide liquids are stable for months in a

nitrogen vacuum desiccator after initial polishing. Sulfide liquids polished/prepared using wet- and oil-based polishing techniques show consistent and substantial halogen loss. Vertical errors represent 2 standard errors on measured concentrations of Br and I.

Fig. 3 Log $\mathrm{D}_{\mathrm{Cl,\ Br,\ I}}^{\mathrm{sul\ liq-sil\ melt}}$ values from this study and Mungall and Brenan (2003) as a function of temperature. Vertical and horizontal errors are errors calculated using simple error propagation and based on 2 standard errors on sulfide liquid and silicate melt abundances of the various halogens.

Fig. 4 Log $\mathrm{D}_{\mathrm{Cl,\ Br,\ I}}^{\mathrm{sul\ liq-sil\ melt}}$ values from this study and Jackson et al. (2018) versus $\mathrm{D}_{\mathrm{O}}^{\mathrm{sul\ liq-sil\ melt}}$ and corresponding empirical polynomial fits for Cl ($\log \mathrm{D}_{\mathrm{Cl}}^{\mathrm{sul\ liq-sil\ melt}} = (-2.5832 * \log \mathrm{D}_{\mathrm{O}}^{\mathrm{sul\ liq-sil\ melt}})^2 - \left(6.2365 * \log \mathrm{D}_{\mathrm{O}}^{\mathrm{sul\ liq-sil\ melt}}\right) - 4.46$; R^2 = 0.56, N = 21), Br ($\log \mathrm{D}_{\mathrm{Br}}^{\mathrm{sul\ liq-sil\ melt}} = (-3.2762 * \log \mathrm{D}_{\mathrm{O}}^{\mathrm{sul\ liq-sil\ melt}})^2 - \left(8.4917 * \log \mathrm{D}_{\mathrm{O}}^{\mathrm{sul\ liq-sil\ melt}}\right) - 5.94$; R^2 = 0.84, N = 7) and I ($\log \mathrm{D}_{\mathrm{I}}^{\mathrm{sul\ liq-sil\ melt}} = (-5.7141 * \log \mathrm{D}_{\mathrm{O}}^{\mathrm{sul\ liq-sil\ melt}})^2 - \left(15.1070 * \log \mathrm{D}_{\mathrm{O}}^{\mathrm{sul\ liq-sil\ melt}}\right) - 9.85$; R^2 = 0.79, N = 7). Vertical and horizontal errors are errors calculated using simple error propagation and based on 2 standard errors on sulfide liquid and silicate melt abundances of the various halogens.

Fig. 5 Halogen concentrations in various calculated reservoirs. Green circles indicate the calculated bulk silicate Earth (BSE) and bulk silicate Mars (BSM) halogen abundances following formation of a 32.5 and 25 mass % terrestrial and martian core (this study, calculated using the bulk Earth and bulk Mars values reported in Table 4, while assuming non-siderophile and non-chalcophile behavior of halogens). Dark blue triangles represent the measured BSE and BSM abundances (taken from Taylor, 2013

and Wang et al.,2018, and references therein). Light blue triangles are the BSE and BSM halogen abundances corrected for extraction of 6 and 20 modal mass % of FeS liquids during accretion of Earth and Mars, respectively (Table 4). In case of the Earth, the abundance of I in the terrestrial mantle was also modeled while incorporating the proposed siderophile behavior of I during core formation ($D_I^{\text{met liq}-\text{sil melt}}$ = 3.4±1.1; Jackson et al., 2018) (indicated by the filled diamond).

Appendix for ''An experimental assessment of the chalcophile behavior of F, Cl, Br and I: implications for the fate of halogens during planetary accretion and the formation of magmatic ore deposits'' by E.S. Steenstra, F. van Haaster, R. van Mulligen, S. Flemetakis, J. Berndt, S. Klemme, W. van Westrenen.

A.1 Electron microprobe analyses of halogens in silicate and sulfide melts

A.1.1. Correction for interferences of F, Br and I with Fe, Al and Ca

It is well established that EPMA measurements of halogens F, Br and I are affected by their interferences with Fe, Al and Ca, respectively. We there used previously determined calibration curves of ''fake'' F, Br and I concentrations for nominally halogen-free silicate melts and sulfides with different FeO and/or Al_2O_3 and/or CaO concentrations. These results yield the following correction curves for F, Br and I concentrations in silicate melts:

F (artificial) ppm in silicate melt = 69.67 * FeO (wt.%) + 280 (R^2 = 0.99) (A.1)

Br (artificial) ppm in silicate melt = 48.05 * Al_2O_3 (wt.%) + 4 (R^2 = 0.99) (A.2)

I (artificial) ppm in silicate melt = 44.25 * CaO (wt.%) + 32 (R^2 = 0.99) (A.3)

For the silicate melt compositions of the experiments reported in this study, these corresponds correspond to corrections of approximately 190 to 900 ppm F, 220 to 600 ppm Br and 150 to 600 ppm I. The calculated ''fake'' concentrations of each of the elements were subtracted from the initially measured concentrations to obtain true abundances of each of the halogens in the silicate melts.

Only Fe is present in significant quantities in the sulfides. We therefore used only the following correction curve for halogen measurements of sulfides:

F (artificial) ppm in sulfide melt = 70.81*Fe (wt.%) + 200 (R^2 = 0.98) (A.4)

This correction corresponds to approximately 4100 to 4400 ppm F and suggests F concentrations in all of the sulfides are below EPMA detection limits.

A.1.2. Low EPMA totals of some experimental run products

The EPMA analyses of several silicate melts yielded low EPMA totals. Low totals of the silicate melt could have been the result of halogens during EPMA analyses. We therefore assessed the potential loss of halogens during EPMA analyses by varying the beam current. The use of both low- and high beam currents yielded Cl and I concentrations within error of each other (0.583±0.004 and 0.554±0.047 wt.% I and 0.055±0.003 and 0.039±0.027 Cl using high (180 nA) and low (20 nA) beam currents, respectively). This confirms that the lower totals of EPMA analyses are not the result of

preferential loss of halogens during the EPMA analysis. Although great care was taken to prevent H_2O contamination of silicate starting materials (storage of powders and prepared piston cylinder assemblies in 110 degree oven), the experiments could have experienced some water contamination due to the hygroscopic nature of halides. However, one would then expect a correlation between halogen content and EPMA totals of the silicate melt (i.e., with increasing halogens lower EPMA silicate melt totals) - which is not observed. This is illustrated by the silicate melt EPMA total of approx. 100% of the most halogen-rich experiment (Fig. S.1). In addition, the silicate melts in metal liquid - silicate melt experiments performed in graphite capsules, in conjunction with the use of talc-pyrex assemblies, do not yield such low totals (Steenstra et al., 2017), suggesting an insignificant role of H_2O contamination. We also reanalyzed some silicate melts after wet-polishing and compared these results with EPMA totals obtained on dry-polished samples. Both totals are similar, suggesting the low totals are not an artifact of dry-polishing (e.g., run FH-8; 97.23±72 (dry) and 97.43±0.48). Low EPMA totals of the silicate melt could also (partly) be a result of incorrect contribution of Fe to FeO*, instead of Fe_2O_3. However, the lack of correlation between the highest FeO* experiments and low totals seem to preclude significant quantities of Fe_2O_3. This agrees with XANES measurements of silicate melts equilibrated in graphite capsules, suggesting reducing conditions of approximately –1 unit below the CCO buffer (e.g., Médard et al., 2015; Ni et al., 2017), with Fe^{3+}/Fe^{total} of <3%. The most likely explanation is therefore a combination of (1) the porous nature of some phases, most notably the quench-textured materials in the sulfides and silicates (see Fig. 1 in main text), (2) the abundances of other trace elements that were not measured, present as impurities in the added Fe-S powder (see Steenstra et al., 2018) and (3) uncertainties related to matrix corrections for the EPMA analyses. In fact, low silicate melt totals seem to be common issue in sulfide liquid-saturated experiments - consideration of the average silicate melt totals of sulfide-saturated experiments in the compiled dataset of Steenstra et al. (2020) (N = 349) yields 98.70±1.61 (1SD). The difficulties of implementing appropiate matrix corrections are likely to be further enlarged by the high halogen contents of the experiments.

A.1.3. Distribution of halogens in the sulfide melts

Relative elemental distribution maps were obtained of I-bearing run products to assess the potential incorporation mechanisms of I, and potentially other halogens, in the sulfide liquid (Fig. S.2–S.5). The results show that high I contents are not well correlated with O contents, or any other compositional parameter. This suggests that I is present in the sulfide liquid as a halide, which may explain the mobile nature of halogens in the sulfide liquid during polishing. The presence of halides is also consistent with the well-defined correlation between I, Br and Cl abundances in the sulfide liquid. Finally, the results show that I abundances do not correlate with lithophile element abundances (e.g., Si, Al), confirming that the measured halogen abundances are not the result of smearing of silicate melt material on the sulfide liquid.

A.2 Predictive equations describing sulfide liquid – silicate melt partitioning of Cl, Br and I

To quantitatively assess which parameters exert the dominant control on $\mathrm{D}_{\mathrm{Cl,\ Br,\ I}}^{\mathrm{sul\ liq-sil\ melt}}$, we first choose to adopt a similar approach to that derived by Kiseeva and Wood (2013, 2015):

$$\log \mathrm{D}_{i}^{\mathrm{sul\ liq-sil\ melt}} = \mathrm{A} + \mathrm{B/T(K)} - \frac{n}{2}\log[\mathrm{FeO}_{\mathrm{sil\ melt}}(\mathrm{wt.\%})] + \varepsilon_{\mathrm{MS}_{n/2}}^{\mathrm{FeO}}\log(1 - x_{\mathrm{FeO}}^{\mathrm{sul\ liq}}) \quad \text{(A.5)}$$

where A and B are regression constants, *T* is temperature in Kelvin, *n* is the valence of element *i* (here assumed to Cl^-, Br^-, I^-) and $x_{\mathrm{FeO}}^{\mathrm{sul\ liq}}$ is the mole fraction of FeO in the sulfide liquid. Term $\varepsilon_{\mathrm{MS}_{n/2}}^{\mathrm{FeO}}$ is a Margules-type of interaction parameter that describes the interaction of element *i* with FeO of the sulfide liquid (Kiseeva and Wood, 2013, 2015).

To assess whether halogen abundances could affect $\mathrm{D}_{\mathrm{Cl,\ Br,\ I}}^{\mathrm{sul\ liq-sil\ melt}}$, we also regressed the data with- and without halogen abundance terms:

$$\log \mathrm{D}_{i}^{\mathrm{sul\ liq-sil\ melt}} = \mathrm{A} + \mathrm{B/T(K)} - \frac{n}{2}\log[\mathrm{FeO}_{\mathrm{sil\ melt}}(\mathrm{wt.\%})] + \varepsilon_{\mathrm{MS}_{n/2}}^{\mathrm{FeO}}\log(1 - x_{\mathrm{FeO}}^{\mathrm{sul\ liq}}) + \mathrm{C} * \mathrm{halogen\ content\ silicate\ melt\ (wt.\%)} \quad \text{(A.6)}$$

Table S.1 show the regression results, obtained using our new data and the data of Jackson et al. (2018) for I for sulfide liquids obtained at 1973 K and 1.5 GPa. The results show that no meaningful statistical fits for Cl and Br can be obtained using this approach, with or without halogen abundance parameters, presumably due to the limited size of both the partition coefficients datasets and ranges of the fit parameters. This also suggest that the variations of $\mathrm{D}_{\mathrm{Cl,\ Br}}^{\mathrm{sul\ liq-sil\ melt}}$ are most readily explained by variations in FeO contents of the silicate liquids and sulfide melts, respectively, and not by variations in *T* or halogen contents of the silicate melts.

Regression results for I suggests that a significant fraction of the variation of $\mathrm{D}_{\mathrm{I}}^{\mathrm{sul\ liq-sil\ melt}}$ may be explained by the I contents of the silicate melt. However, it is currently unclear whether this is purely a result of correlation between $\mathrm{D}_{\mathrm{I}}^{\mathrm{sul\ liq-sil\ melt}}$ and I contents of the silicate melt. The experiments of Jackson et al. (2018) have the lowest

O contents (0.49–1.01 wt.%) of all of the sulfide liquids considered for I in this study, but also the highest I contents (1.87–2.93 wt.%). The regressions also suggest temperature may decrease $D_I^{sul\ liq-sil\ melt}$, but the experimental *T* range is also limited (1683–1973 K).

Supplementary references

Jackson C.R.M., Bennett N.R., Du Z., Cottrell E., Fei Y. (2018) Early episodes of high-pressure core formation preserved in plume mantle. *Nature* **553**, 491–495.

Kiseeva E.S., Wood B.J. (2013) A simple model for chalcophile element partitioning between silicate and sulphide liquids with geochemical applications. *Earth Planet. Sci. Lett.* **383,** 68–81.

Kiseeva E.S., Wood B.J. (2015) The effects of composition and temperature on chalcophile and lithophile element partitioning into magmatic sulphides. *Earth Planet. Sci. Lett.* **424**, 280–294.

Médard E., McCammon C.A., Barr J.A., Grove T.L. (2008) Oxygen fugacity, temperature reproducibility, and H2O contents of nominally anhydrous piston-cylinder experiments using graphite capsules. *Am. Mineral.* **93(11–12)**, 1838–1844.

Ni P., Zhang Y., Fiege A., Newville M., Lanzirotti A. (2017) Rapid reduction of MORB glass in piston cylinder experiments with graphite capsules – a XANES study. *AGU* #V11B–0342 (abstr.).

Steenstra E.S., Sitabi A.B., Lin Y.H., Rai N., Knibbe J.S., Berndt J., Matveev S., van Westrenen W. (2017) The effect of melt composition on metal-silicate partitioning of siderophile elements and constraints on core formation in the angrite parent body. *Geochim. Cosmochim. Acta* **212**, 62–83.

Steenstra E.S., Seegers A.X., Eising J., Tomassen B.G.J., Webers F.P.F., Berndt J., Klemme S., Matveev S., van Westrenen W. (2018) Evidence for a sulfur-undersaturated lunar interior from the solubility of sulfur in lunar melts and sulfide-silicate partitioning of siderophile elements. *Geochim. Cosmochim. Acta* **231**, 130–156.

Steenstra E.S., Berndt J., Klemme S., Rohrbach A., Bullock E.S., van Westrenen W. (2020) An experimental assessment of the potential of sulfide saturation of the source regions of eucrites and angrites: implications for asteroidal models of core formation, late accretion and volatile element depletions. *Geochim. Cosmochim. Acta* **269,** 39–62.

Fig. S.1: EPMA-derived silicate melt totals as a function of FeO* (upper panel) and total halogen content of the silicate melt (lower panel). The absence of a correlation between EPMA totals and FeO* of the silicate melt suggests that it is unlikely the EPMA total deficiency is the result of the presence of Fe_2O_3. The lack of correlation between the EPMA totals and total halogen contents excludes loss of halogens under the EPMA beam as a major contributor to the low totals of the silicate melt, as well as potential H_2O contamination.

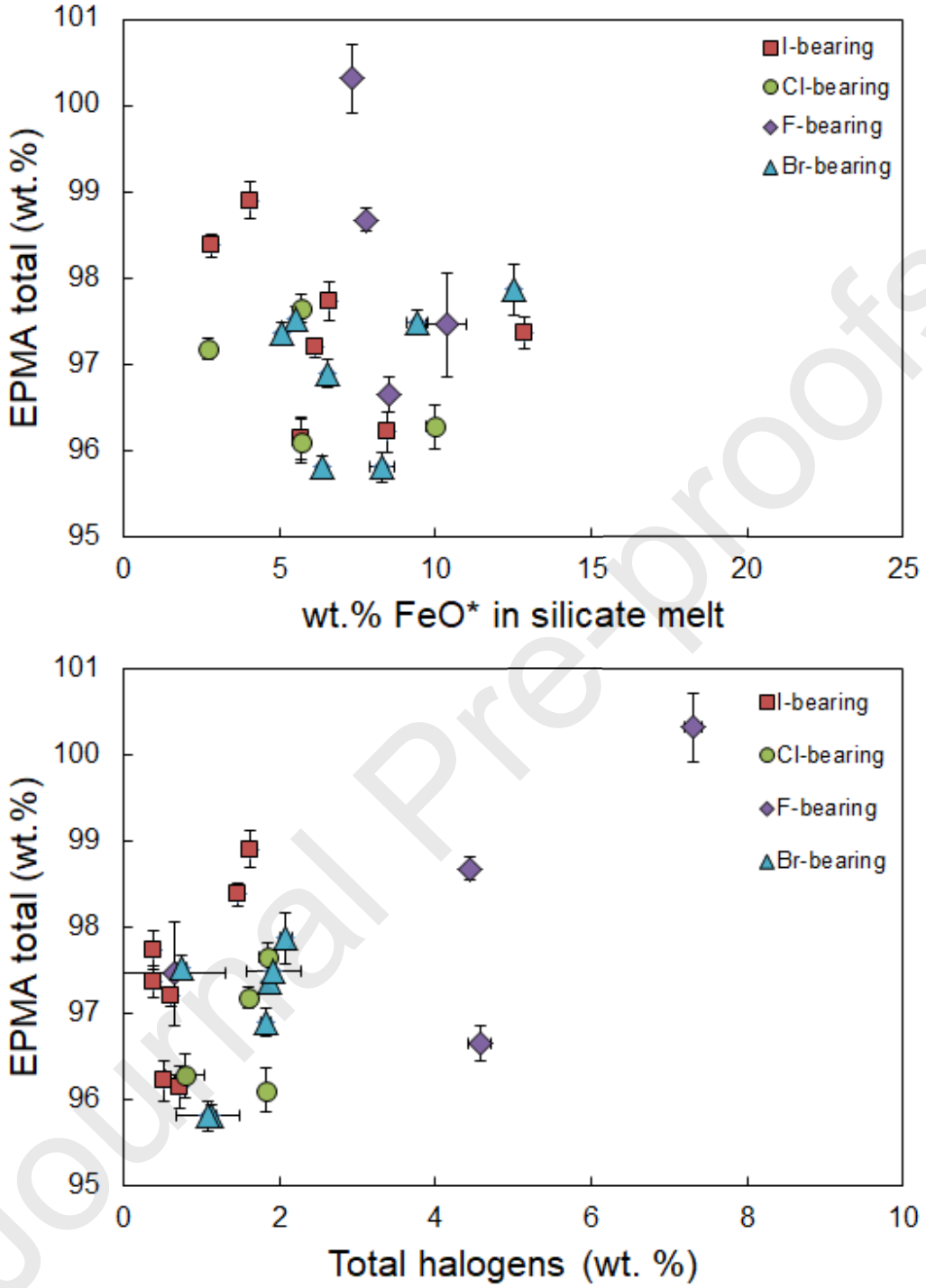

Fig. S.2: Relative elemental distribution maps obtained by EPMA for run I-FeS-3.

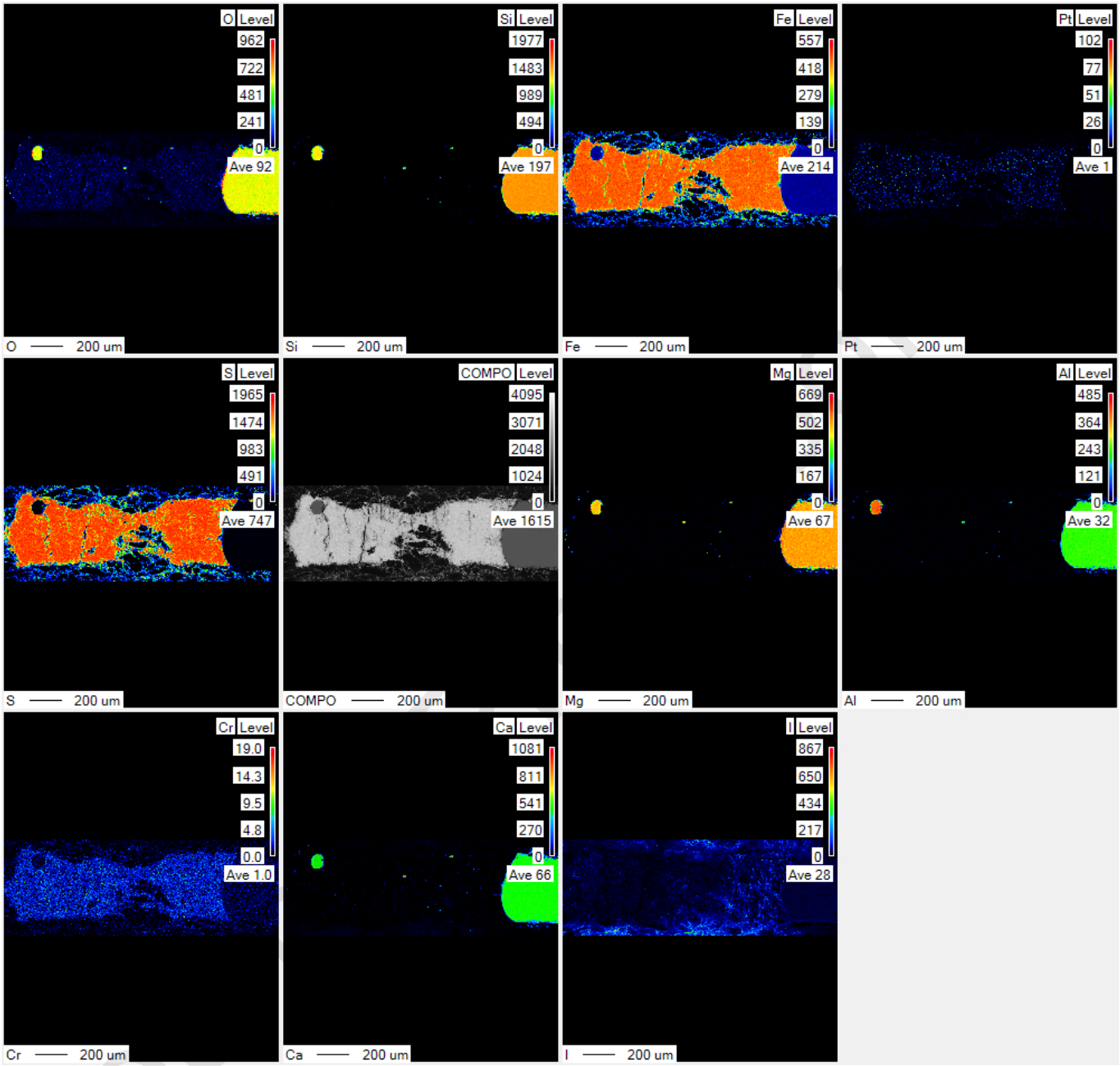
O Level
962
722
481
241
0
Ave 92
O 200 um
Si Level
1977
1483
989
494
0
Ave 197
Si 200 um
Fe Level
557
418
279
139
0
Ave 214
Fe 200 um
Pt Level
102
77
51
26
0
Ave 1
Pt 200 um
S Level
1965
1474
983
491
0
Ave 747
S 200 um
COMPO Level
4095
3071
2048
1024
0
Ave 1615
COMPO 200 um
Mg Level
669
502
335
167
0
Ave 67
Mg 200 um
Al Level
485
364
243
121
0
Ave 32
Al 200 um
Cr Level
19.0
14.3
9.5
4.8
0.0
Ave 1.0
Cr 200 um
Ca Level
1081
811
541
270
0
Ave 66
Ca 200 um
I Level
867
650
434
217
0
Ave 28
I 200 um

Fig. S.3: Relative eemental distribution maps of the sulfide liquid of run I-FeS-3 obtained by EPMA.

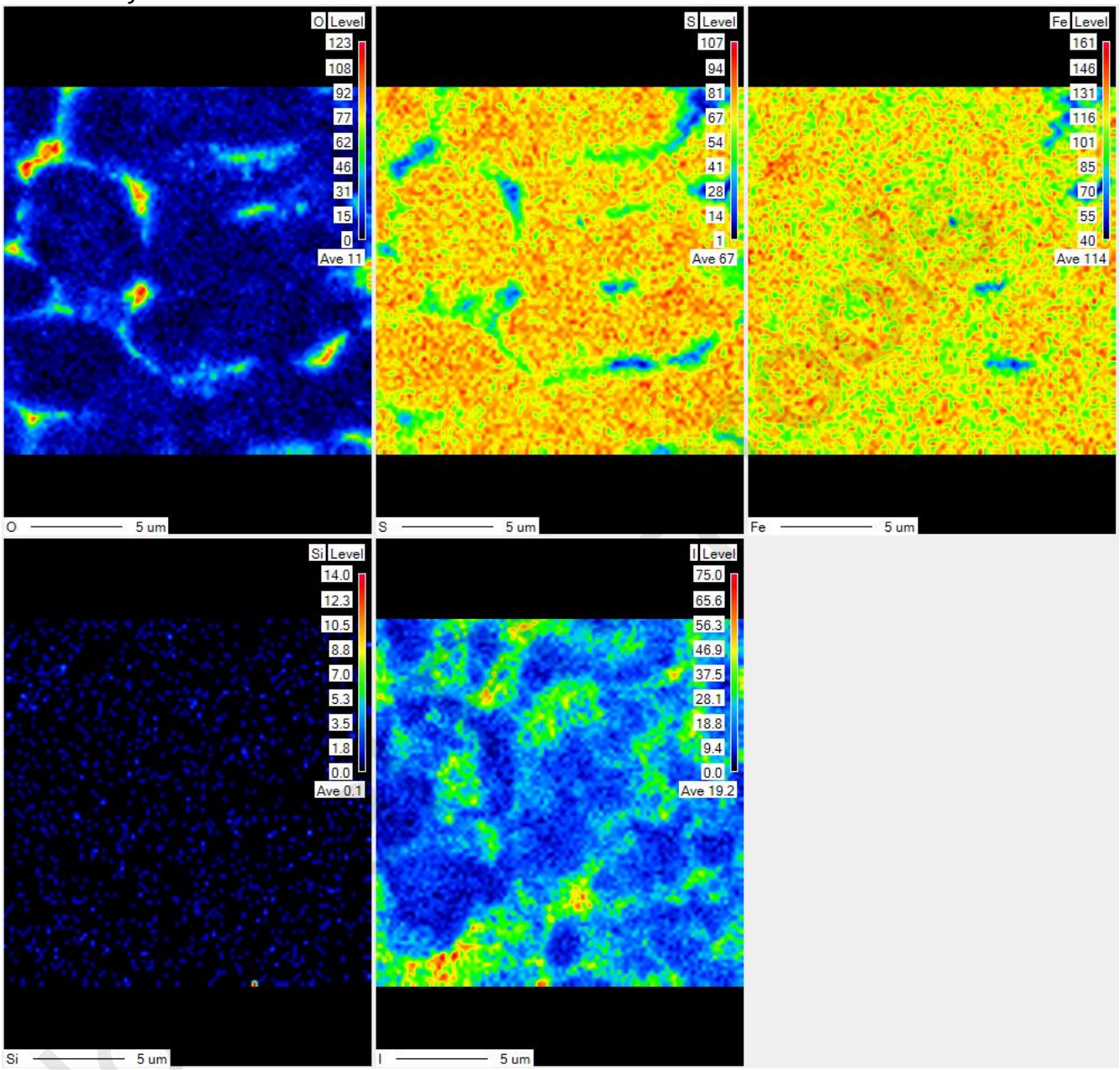

Fig. S.4: Relative elemental distribution maps obtained by EPMA for run I-FeS-2.

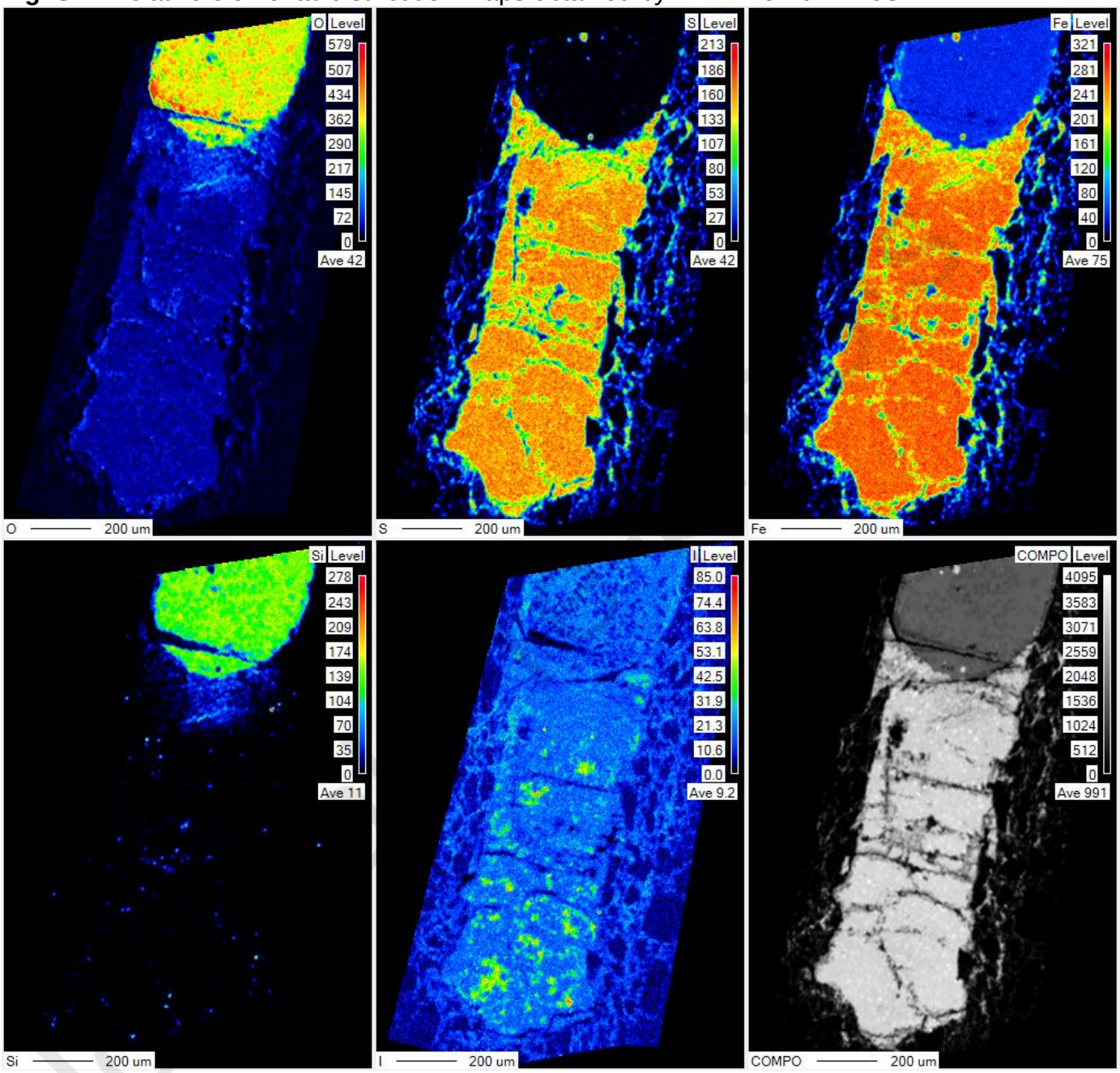

Fig. S.5: Relative elemental distribution maps obtained by EPMA for run I-FeS-2.

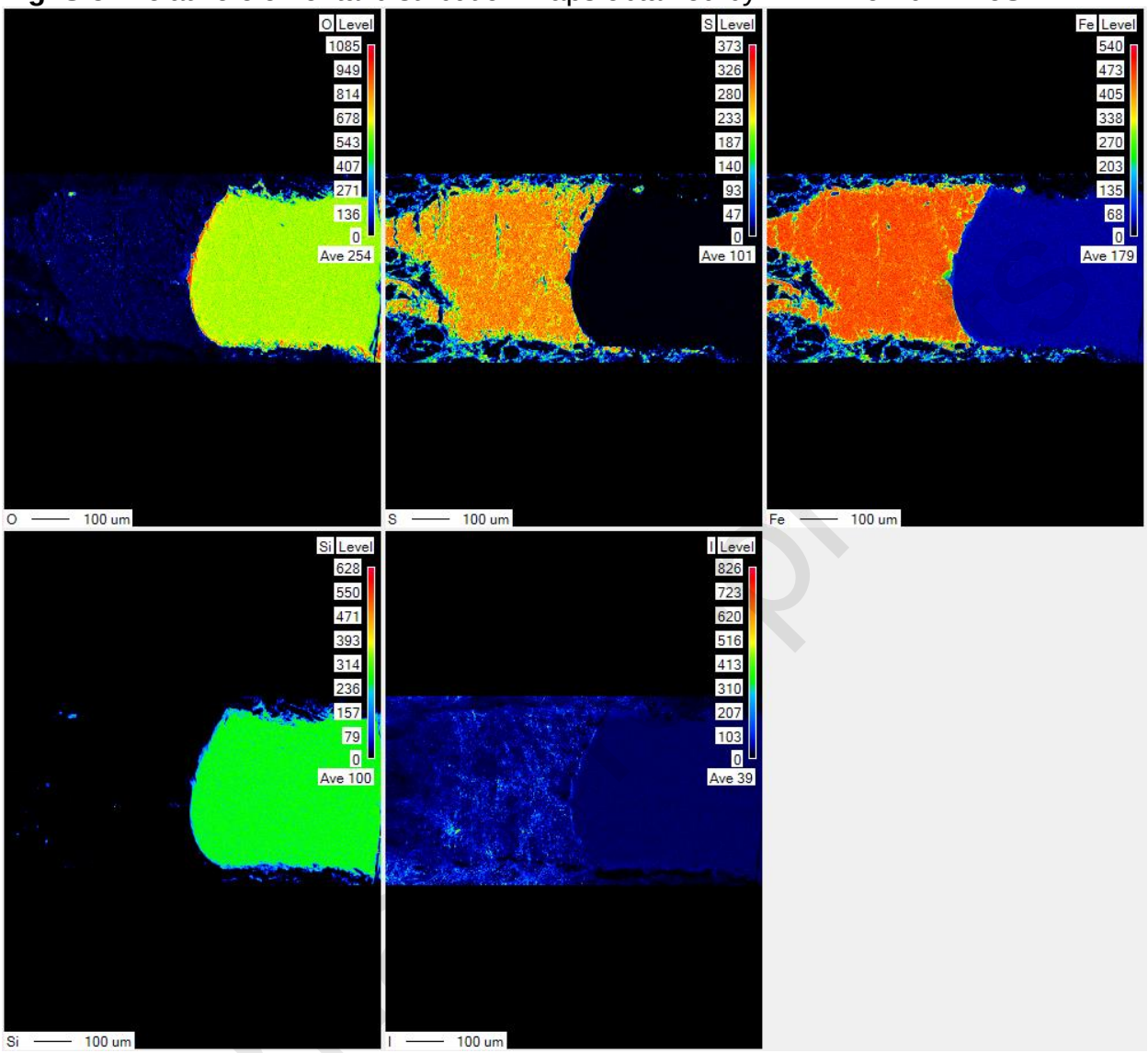

Fig. S.6: Correlation of Cl in sulfide liquid versus I and Br contents of experimental run products.

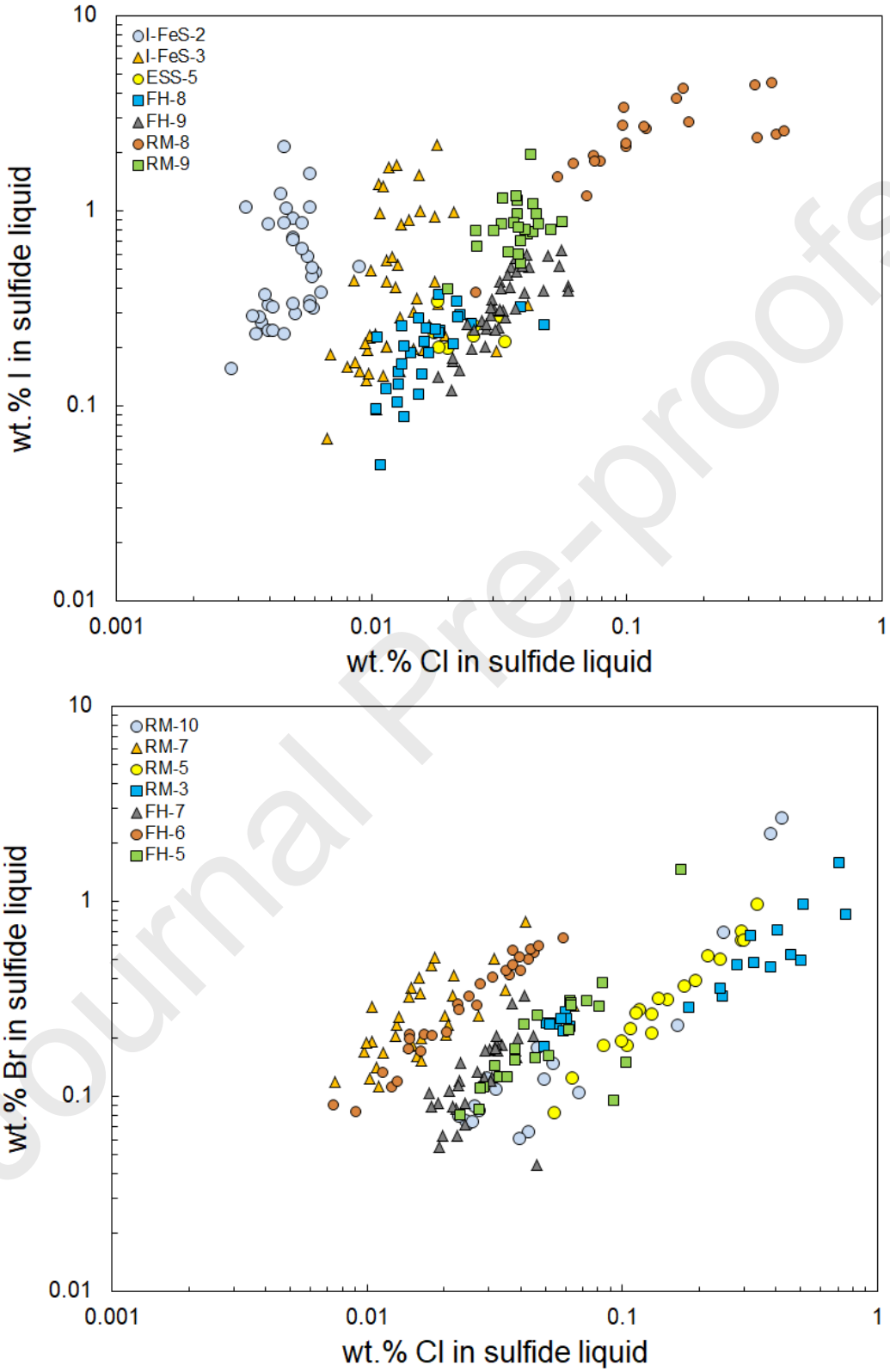

Fig. S.7: % deviation of post-experimental measured bulk halogens, compared to initial added abundances, plotted as a function of run time at 1683 K (top panel) and peak temperature (middle panel). Also shown is the absence of a correlation between log D values and the inferred extent of halogen loss (lower panel). Horizontal solid orange and dashed red lines indicate the average ranges of deviations in post-experimental halogen bulk abundances, compared to initial added abundances, for I and Br, respectively (Table S.1).

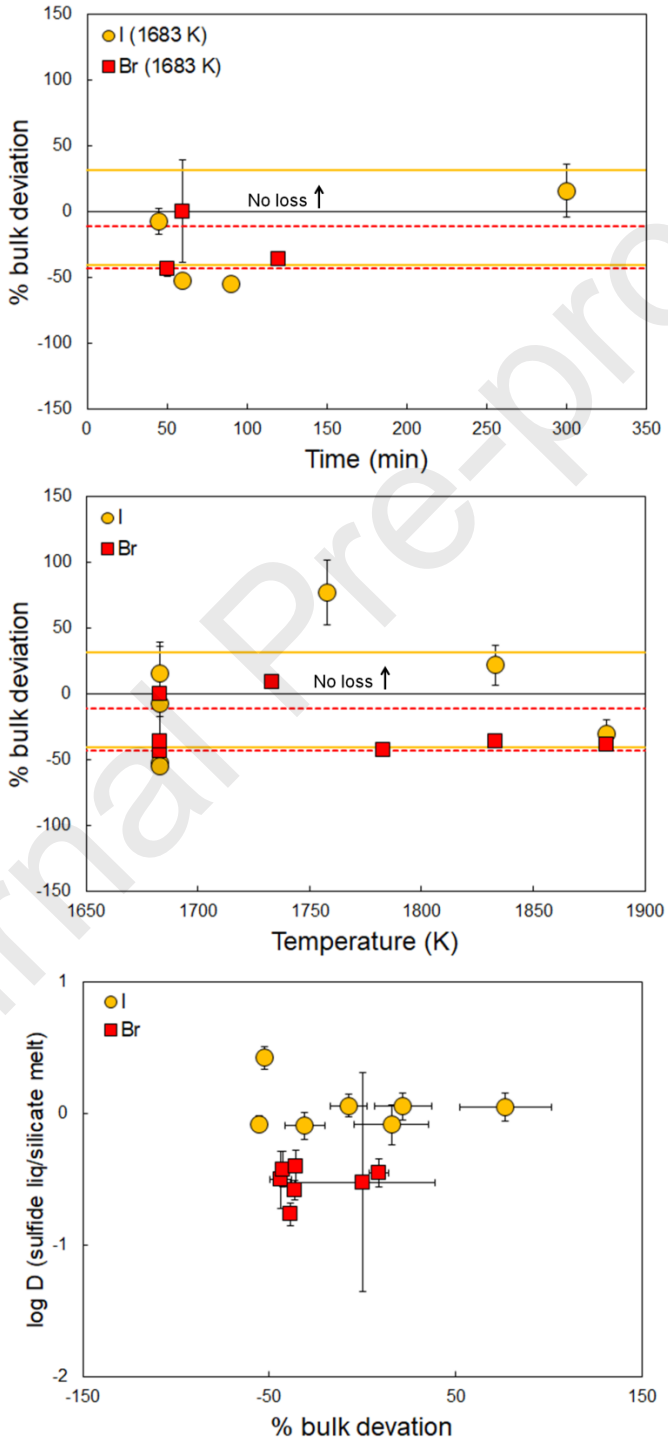

Table S.1 Added and estimated abundances of halogens in experimental run products

	T (K)	t (min)	Composition	Initial bulk abundance (added)	Initial bulk abundance (based on K)	Bulk abundance after experiment	% deviation bulk halogen abundances after experiment
Iodine							
I-FeS-2	1758	300	GG + 2 wt.% I	0.90	0.73	1.29±0.18	+77±25
I-FeS-3	1683	300	GG + 2 wt.% I	1.00	0.90	1.04±0.18	+16±20
ESS-5	1833	60	GG + 2 wt.% I	0.80	0.65	0.79±0.10	–22±15
FH-8	1883	15	GG + 2 wt.% I	0.90	0.84	0.58±0.09	–31±11
FH-9	1683	45	GG + 2 wt.% I	0.80	0.82	0.76±0.08	+7±10
RM-9	1683	90	GG + 2 wt.% I	1.70	2.17	0.97±0.02	–55±1
RM-8	1683	60	GG + 2 wt.% I	1.70	2.40	1.14±0.09	–53±4
							AVG: –5(36)
Chlorine							
ESS-7	1683	90	GG + 1 wt.% Cl	0.75	0.89	1.25±0.07	+40±8
FH-2	1683	120	GG + 1 wt.% Cl	0.40	0.71	1.51±0.06	+113±8
FH-4	1783	60	GG + 1 wt.% Cl	0.15	0.16	1.53±0.18	+856±113[a]
RM-11	1683	60	GG + 1 wt.% Cl	0.60	0.95	1.62±0.06	+71±6
							AVG: +75(42)
Fluorine							
RM-1	1683	60	GG + 4 wt.% F	3.40	–	5.39±0.60	+59±18
RM-2	1683	120	GG + 4 wt.% F	3.40	–	3.17±0.07	–7±2
FH-3	1683	30	GG + 1 wt.% F	0.70	–	0.68±0.34	–3±49
RM-6	1783	30	GG + 4 wt.% F	3.20	–	3.76±0.06	+18±2
							AVG: +17(30)
Bromine							
FH-5	1683	50	GG + 2 wt.% Br	1.20	1.59	0.89±0.09	–44±6
FH-6	1733	45	GG + 2 wt.% Br	1.00	1.14	1.24±0.06	+9±5
FH-7	1833	30	GG + 2 wt.% Br	1.20	0.99	0.63±0.01	–36±1
RM-3	1783	45	GG + 2 wt.% Br	1.80	1.98	1.13±0.02	–43±1
RM-5	1683	120	GG + 2 wt.% Br	1.70	1.33	0.85±0.03	–36±2
RM-7	1883	15	GG + 2 wt.% Br	1.70	2.72	1.67±0.03	–39±1
RM-10	1683	60	GG + 2 wt.% Br	1.50	1.24	1.24±0.48	0±39
							AVG: –27(16)

[a] Uncertain determination of modal abundances of each phase and excluded from average

Table S.2 Multilinear regression results obtained using Eqs. (A.5, A.6)

	A	B (1/*T* (K))	$\varepsilon_{\mathrm{MS}_{n/2}}^{\mathrm{FeO}}$	wt.% Cl	wt.% Br	wt.% I	R^2	N [a]	Refs.
$\log \mathrm{D}_{\mathrm{Cl}}^{\mathrm{sul\ liq-sil\ melt}}$ (Eq. A.5)	n.s.s.	n.s.s.	n.s.s.	–	–	–	–	21	1
$\log \mathrm{D}_{\mathrm{Cl}}^{\mathrm{sul\ liq-sil\ melt}}$ (Eq. A.6)	–1.13(7)	n.s.s.	n.s.s.	–0.22(8)	–	–	0.26	21	1
$\log \mathrm{D}_{\mathrm{Br}}^{\mathrm{sul\ liq-sil\ melt}}$ (Eq. A.5)	n.s.s.	n.s.s.	n.s.s.	–	–	–	–	7	1
$\log \mathrm{D}_{\mathrm{Br}}^{\mathrm{sul\ liq-sil\ melt}}$ (Eq. A.6)	n.s.s.	n.s.s.	n.s.s.	–	n.s.s.	–	–	7	1
$\log \mathrm{D}_{\mathrm{I}}^{\mathrm{sul\ liq-sil\ melt}}$ (Eq. A.5)	–9.51(134)	15155(2392)	–27(10)	–	–	–	0.89	9	1, 2
$\log \mathrm{D}_{\mathrm{I}}^{\mathrm{sul\ liq-sil\ melt}}$ (Eq. A.6)	–6.28(166)	10696(2857)	n.s.s	–	–	–0.32(12)	0.90	9	1 ,2

[a] Number of measurements included in regression. **References:** [1] This study [2] Jackson et al. (2018)

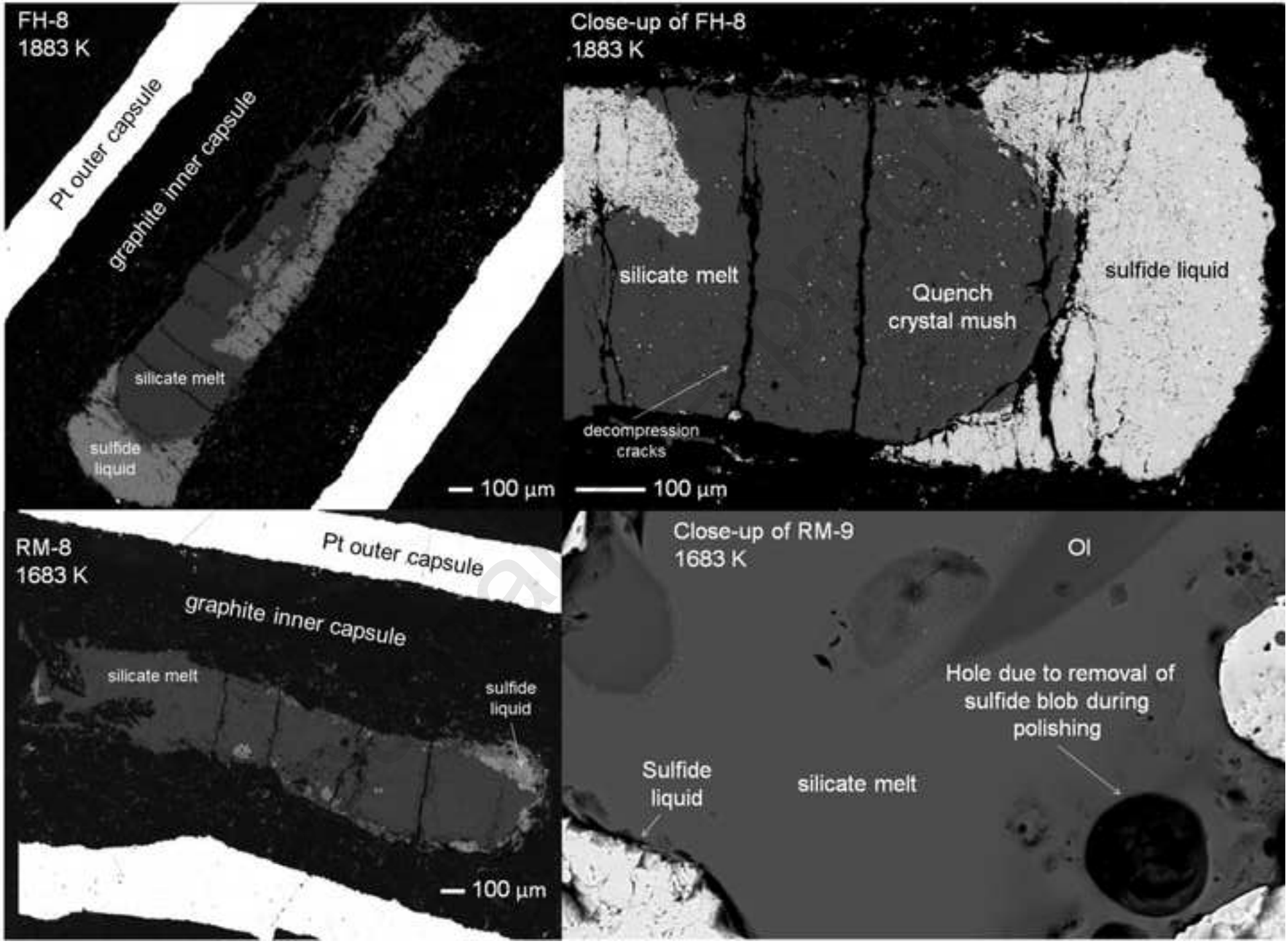
FH-8
1883 K
Pt outer capsule
graphite inner capsule
silicate melt
sulfide liquid
100 µm
Close-up of FH-8
1883 K
silicate melt
Quench crystal mush
sulfide liquid
decompression cracks
100 µm
RM-8
1683 K
Pt outer capsule
graphite inner capsule
silicate melt
sulfide liquid
100 µm
Close-up of RM-9
1683 K
Ol
Hole due to removal of sulfide blob during polishing
Sulfide liquid
silicate melt

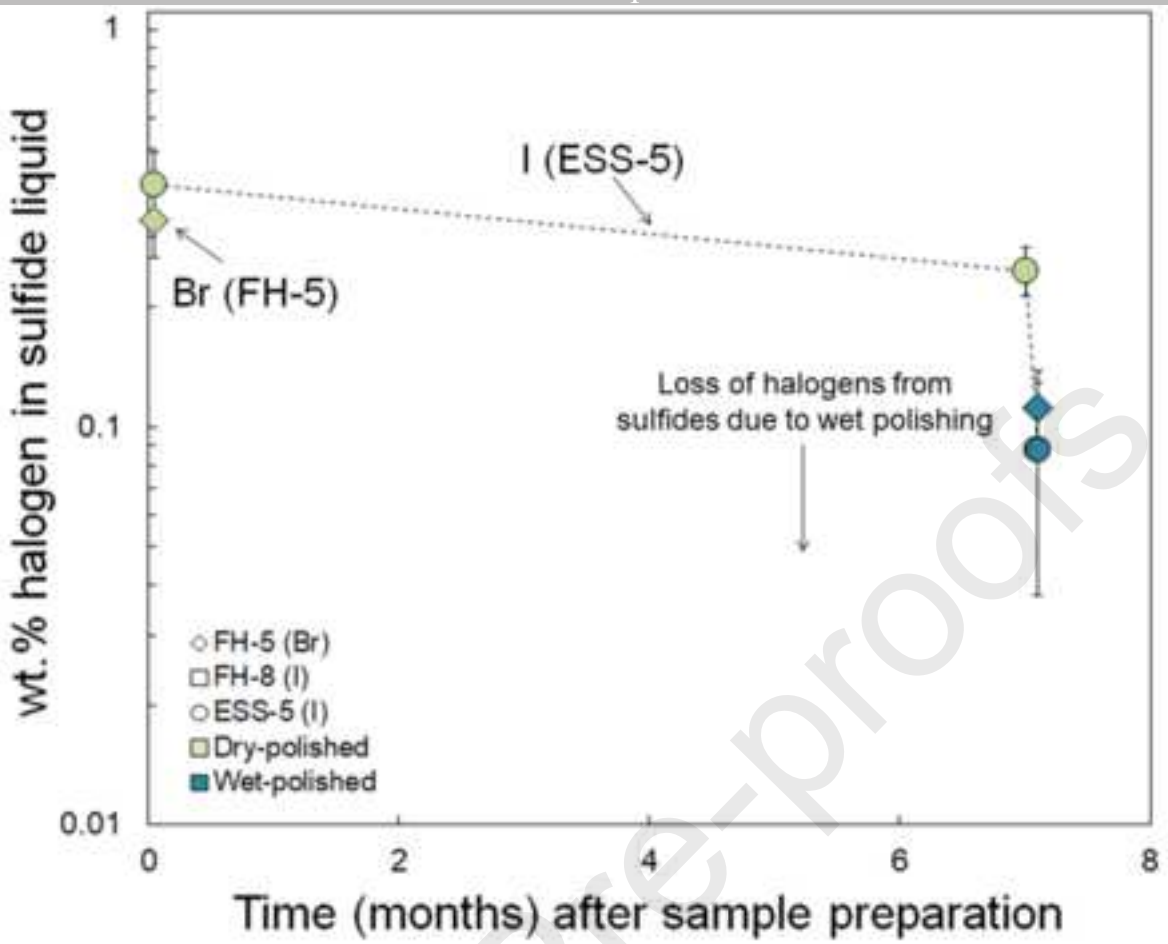

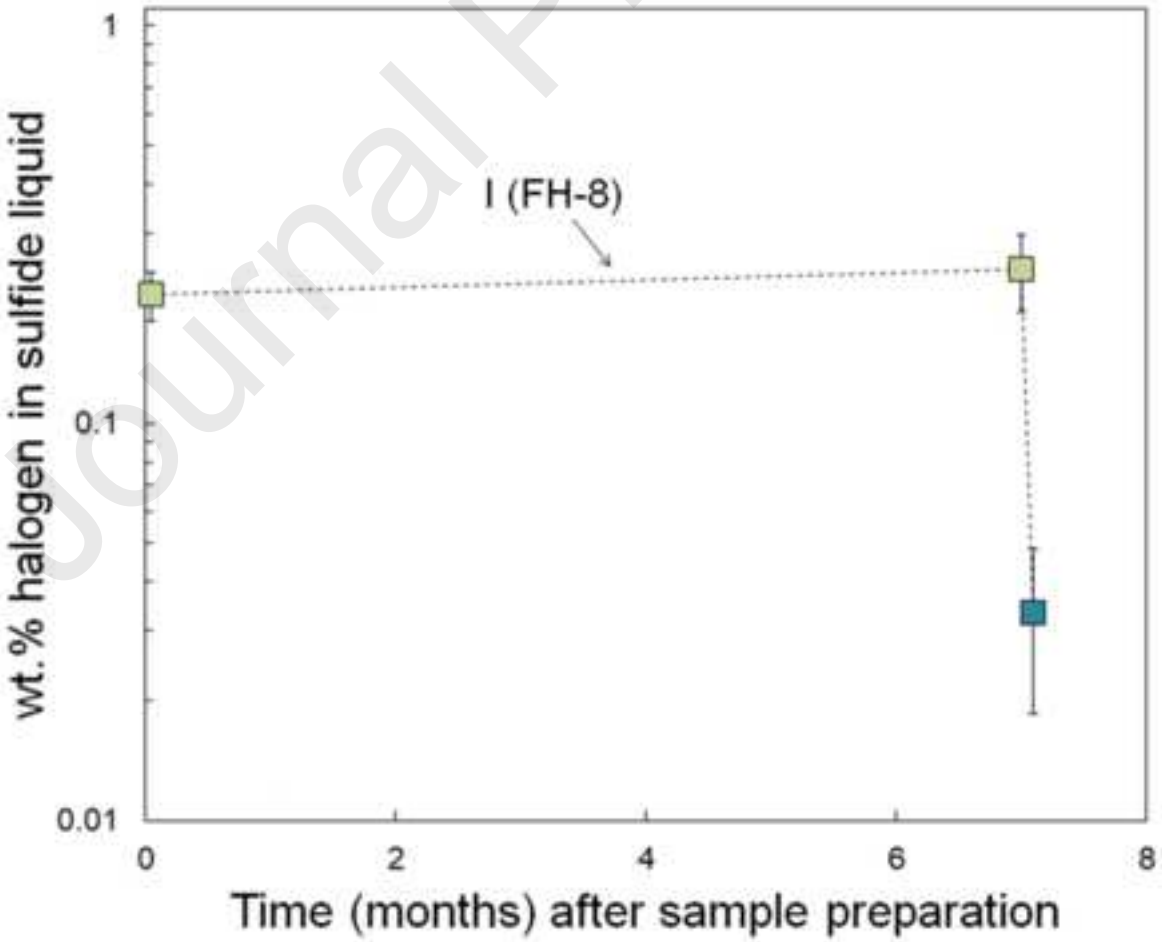

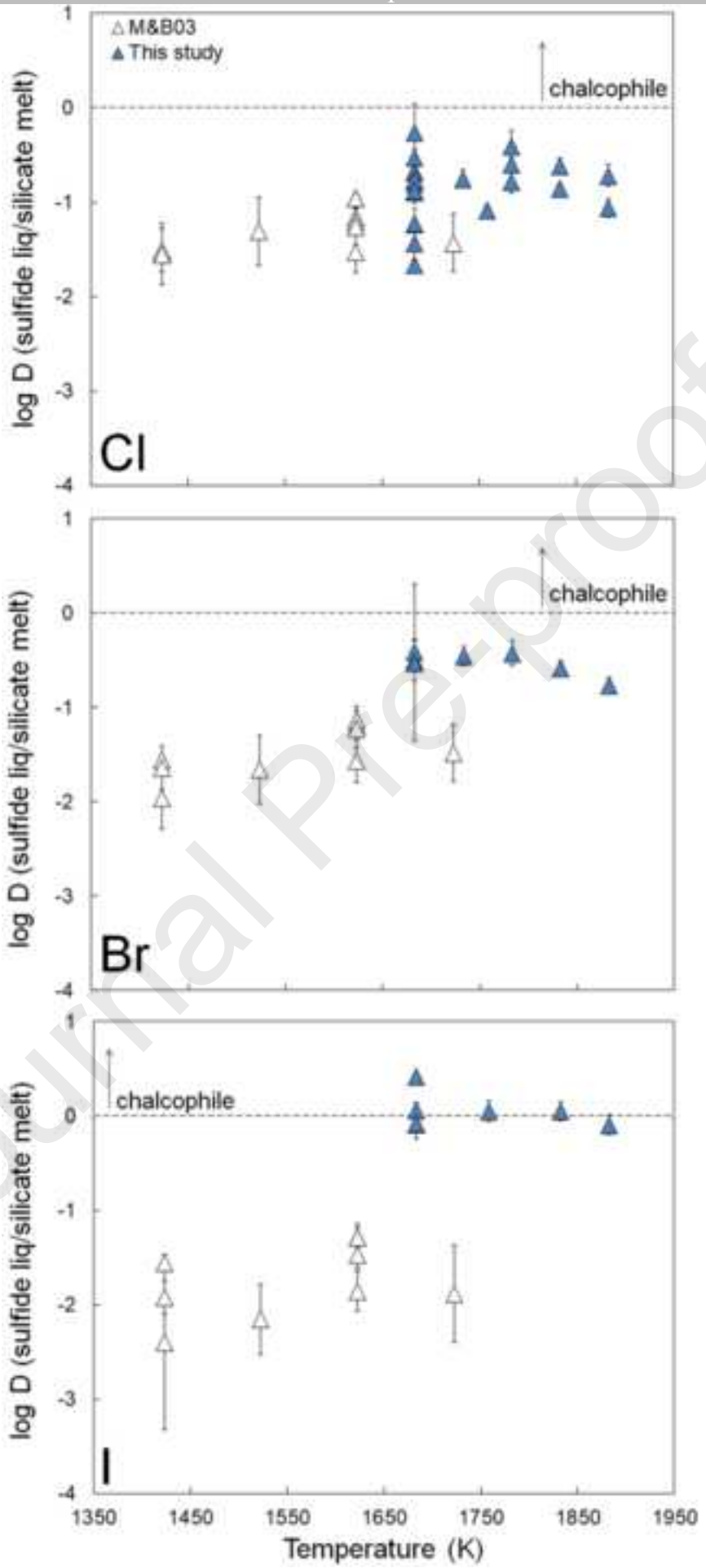

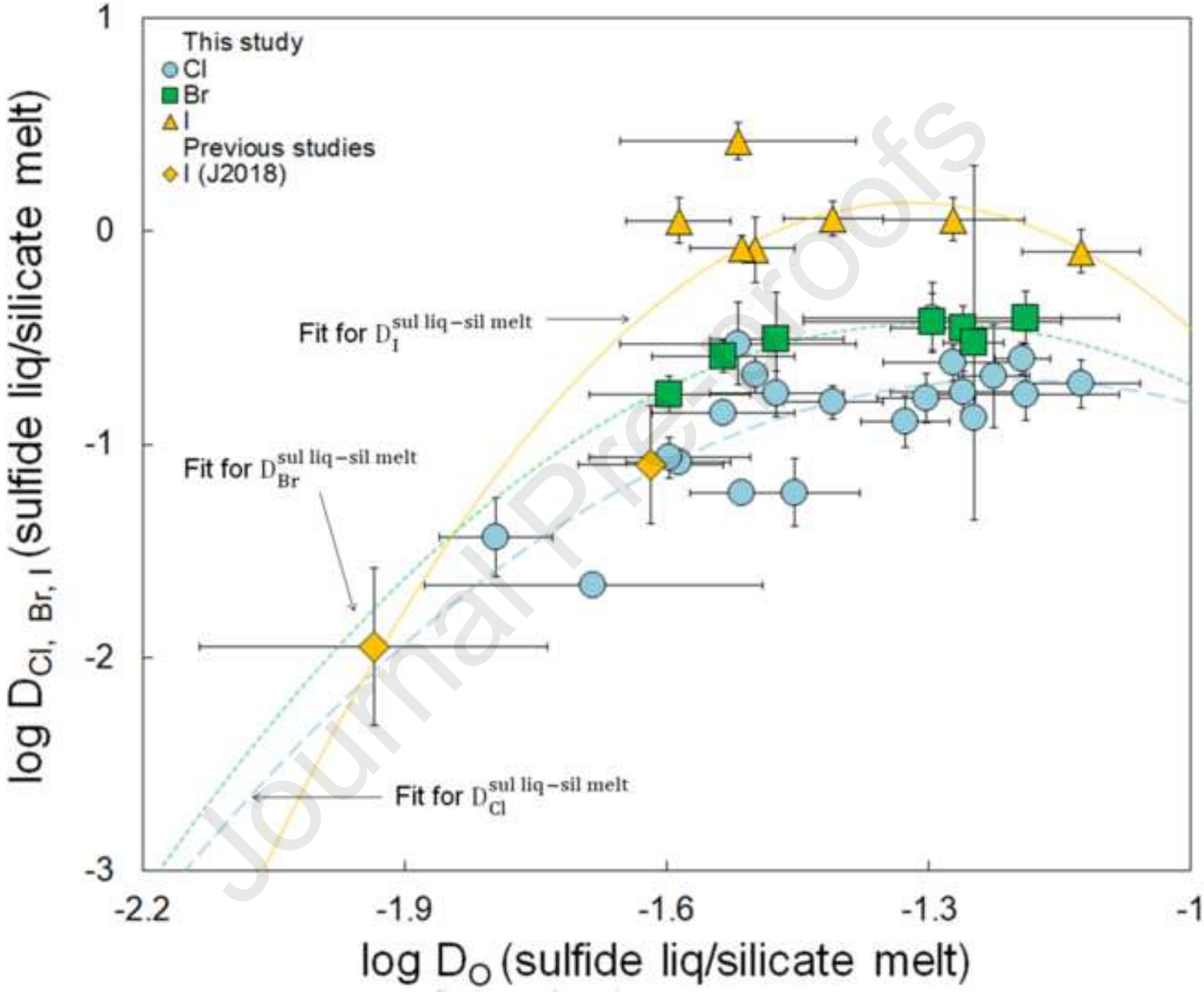

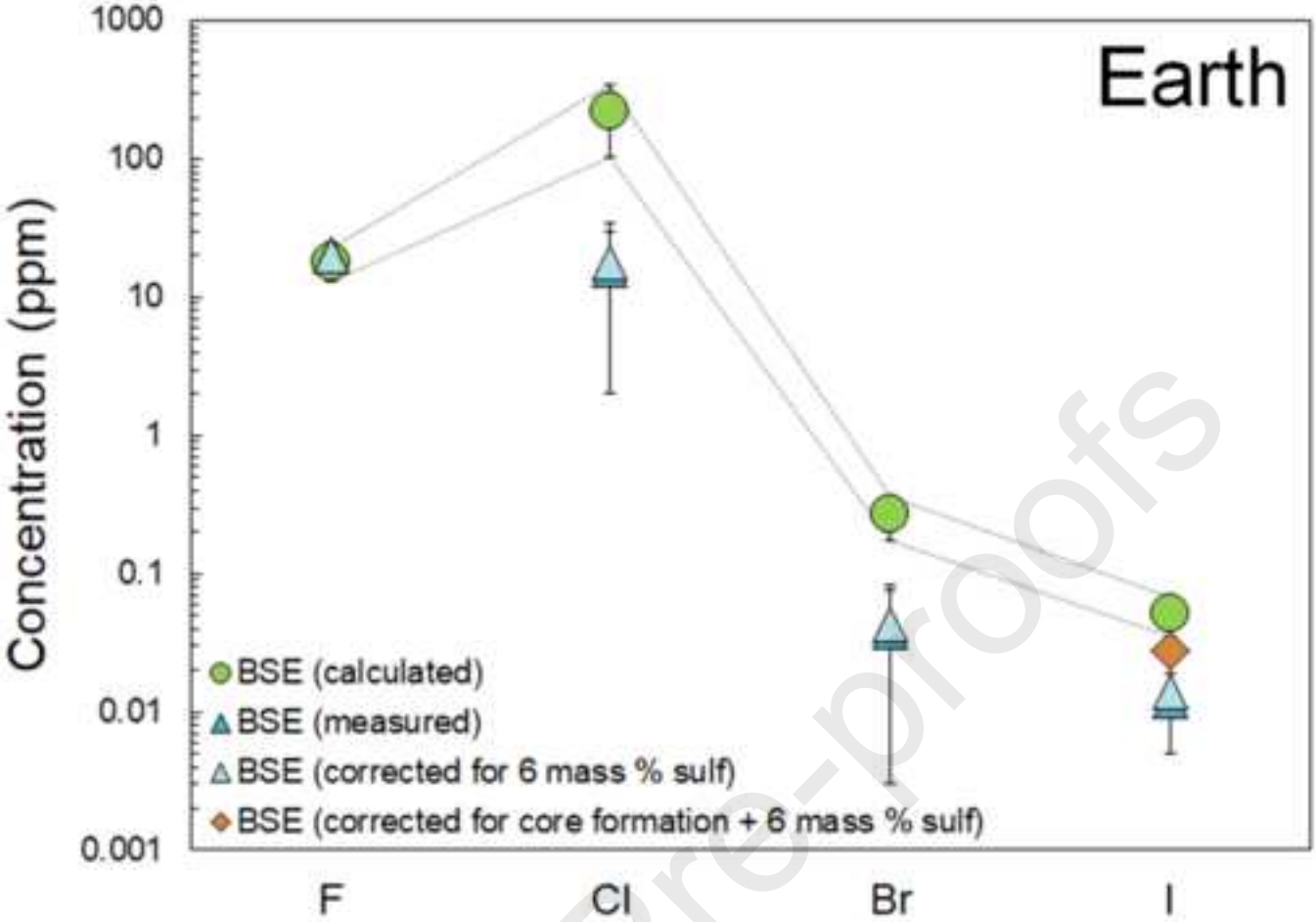

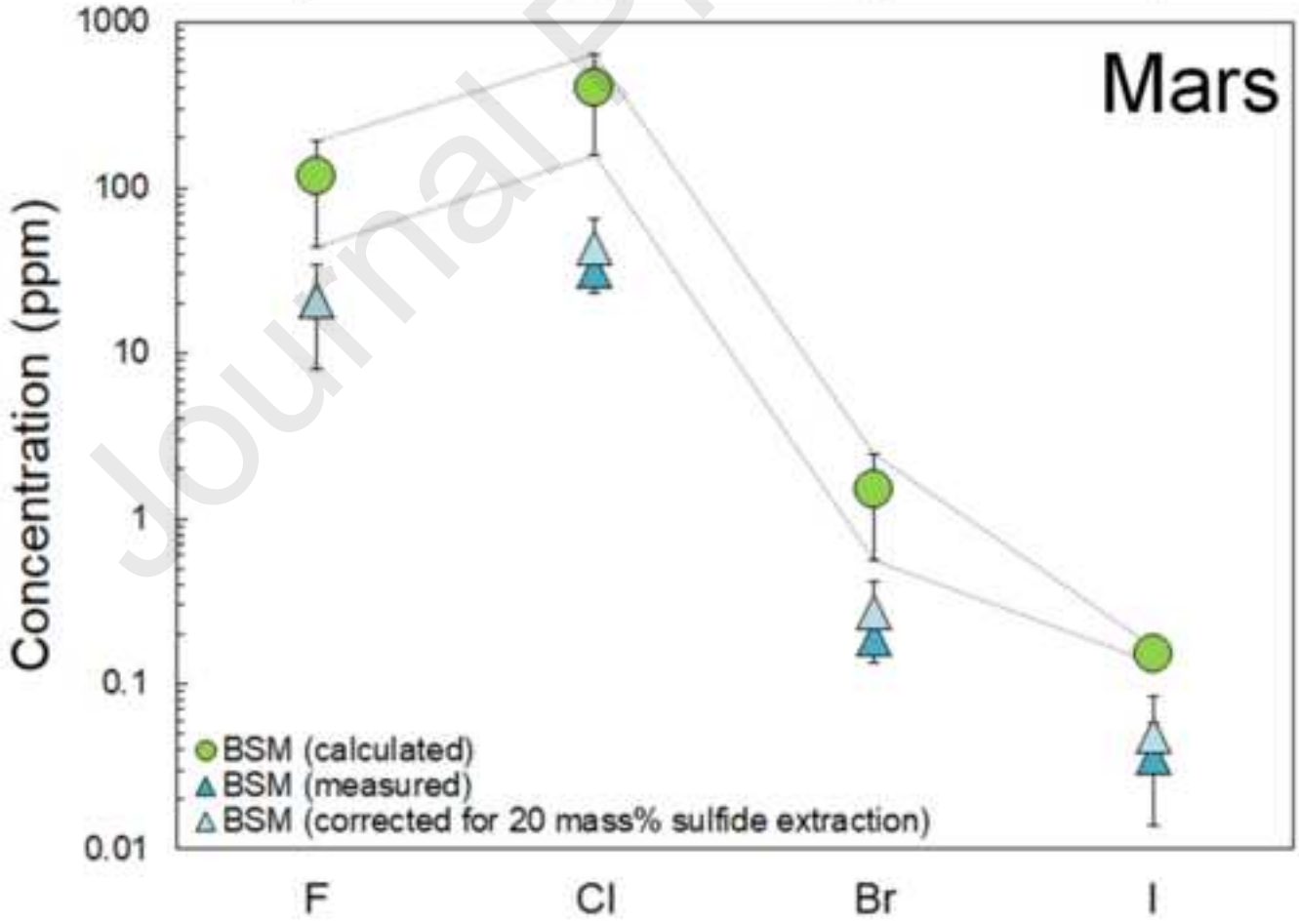

- Dry-polishing is crucial for obtaining accurate halogen contents of sulfide alloys
- Cl, Br and I behave increasingly chalcophile with increasing ionic radius
- Cl, Br and I behave increasingly chalcophile with increasing sulfide O content
- Sulfide liquid segregation did not significantly affect halogen abundances

Declaration of interests

☒ The authors declare that they have no known competing financial interests or personal relationships that could have appeared to influence the work reported in this paper.

☐The authors declare the following financial interests/personal relationships which may be considered as potential competing interests: